Embedded UAV Model and LASER Aiding Techniques for High Accuracy Inertial Navigation Systems

J.F. Vasconcelos*, C. Silvestre, P. Oliveira, B. Guerreiro

Institute for Systems and Robotics, Instituto Superior Técnico, Lisbon, Portugal

Abstract

This work proposes two aiding techniques to enhance the performance of inertial navigation systems (INS), for precise maneuvering of Uninhabited Air Vehicles (UAVs). An embedded methodology to exploit the vehicle dynamics (VD) in the navigation system is proposed, that integrates the vehicle information directly in the Extended Kalman Filter state model. The embedded VD and the INS algorithm propagate simultaneously the inertial states, allowing for the estimation of the INS errors by exploiting the information enclosed in the vehicle dynamics. Attitude, velocity and inertial sensors bias estimates are enhanced by the states predicted by the VD. The proposed technique reduces some of computational routines associated with VD aiding, with an accuracy equivalent to that of the classical technique. A LASER range finder sensor is also integrated in the navigation system to provide high precision distance-to-ground readings for critical takeoff and landing maneuvers. Simulation results for the nonlinear dynamics of a Vario X-Treme model-scale helicopter are presented and discussed. Attitude and position estimation results evidence that the proposed techniques are a valuable navigation aiding solution for UAVs maneuvering in mission scenarios with limited GPS availability and/or high accuracy requirements.

Key words: Inertial navigation, Extended Kalman filter, Vehicle dynamic model, Sensor fusion, Vertical take off and landing

1. Introduction

The latest technological developments bring about Uninhabited Air Vehicles (UAVs) as versatile, multipurpose platforms able to perform a wide variety of missions. The vast scope of practical applications ranges from coastal surveillance, bridge monitoring, traffic watch, to domestic security, and search and rescue missions in extreme environments. Among the existing air vehicles, model-scale helicopters step forward

*Institute for Systems and Robotics (ISR), Instituto Superior Técnico (IST), Av. Rovisco Pais, 1, Torre Norte, 8° Andar, 1049-001, Lisbon, Portugal. Tel: (+351) 21-8418054, Fax: (+351) 21-8418291.

Email addresses: jfvasconcelos@isr.ist.utl.pt (J.F. Vasconcelos), cjs@isr.ist.utl.pt (C. Silvestre), pjcro@isr.ist.utl.pt (P. Oliveira), bguerreiro@isr.ist.utl.pt (B. Guerreiro)

as a challenging platform with the ability to perform Vertical Takeoff and Landing (VTOL), featuring high maneuverability and complex, fast open-loop unstable dynamics.

To satisfy time enduring mission requirements, these vehicles are usually equipped with ultra light weight, low-cost navigation systems, designed for high performance and robustness. However, low-cost sensor units are affected by non-idealities, such as bias and noise, that hinder the required accuracy, but can be tackled by introducing additional data sources. This motivates the development of advanced filtering techniques that exploit aiding measurements and the available information about the UAV.

Vehicle model aiding can be adopted in virtually any application where the vehicle dynamics are known. It is of interest in indoor applications, urban scenarios, or hostile environments, where other aiding sensor can be inoperative or subject to jamming or distortion. Vehicle dynamics are a software based solution that provides information about the UAV motion, and is combined with the inertial navigation estimates using filtering techniques. The integration of vehicle model with the inertial system kinematics allows for the compensation of inertial estimation errors, bearing performance improvements on state variables that are critical for precise maneuvering.

This paper discusses and proposes advanced aiding techniques for precise UAV position and attitude estimation using low-cost sensors. The navigation system architecture is based on merging a high accuracy inertial navigation system (INS) with the information obtained from the vehicle dynamics (VD), using an Extended Kalman Filter (EKF). A new method to integrate the vehicle model in the navigation system is proposed, based on using the vehicle dynamics to propagate the INS state estimates, exploiting the redundancy of the VD and the INS algorithms. Whereas classical methods integrate a full state vehicle simulator and require the estimation and compensation of the vehicle model errors, the new method integrates the VD directly in the EKF to estimate exclusively the INS errors. The proposed VD aiding method allows for the decoupling of the vehicle model differential equations, and selection of those describing the vehicle more accurately. A LASER range finder sensor implementation for takeoff and landing operations is also detailed, enhancing the vertical channel position and velocity estimates. The VD and LASER aiding techniques are demonstrated for a Vario X-Treme helicopter dynamic model, and the accuracy enhancements for takeoff, cruise and landing operations are evidenced in simulation.

The INS is a dead-reckoning algorithm that computes attitude, velocity and position based on the inertial sensor readings. High precision INS algorithms that account for high frequency attitude, velocity and position motions (denoted as coning, sculling and scrolling respectively) are developed in (Savage, 1998a,b; Ignagni, 1998). The inertial attitude, velocity and position estimates are affected by inertial sensor biases and noise, and filtering techniques such as the EKF are adopted to dynamically compensate for non-ideal sensor characteristics that otherwise yield unbounded INS errors. Theory and application related to the EKF and INS algorithms can be found in (Brown and Hwang, 1997; Crassidis et al., 2007; Kinsey et al., 2006;

Dissanayake and Sukkarieh, 2001; Koifman and Bar-Itzhack, 1999) and in references therein.

Classical GPS/INS navigation strategies comprising inertial sensor biases estimation are found to hold only partial observability for a time-invariant configuration, as discussed in (Goshen-Meskin and Bar-Itzhack, 1992a,b). The observability of position, attitude, and sensor non-idealities can be enhanced by introducing vehicle model information.

Simple motion constraints have been successfully implemented in the past for land vehicle applications, by introducing the concept of virtual observations, see (Bryson and Sukkarieh, 2004; Ma et al., 2003; Dissanayake and Sukkarieh, 2001). Nonholonomic constraints of wheeled vehicles, namely the inability to takeoff or perform lateral translation, are exploited in the navigation system by inputting zero valued virtual measurements of the body frame y and z axes velocity. Also, vehicle dynamics bandwidth information and frequency contents are successfully implemented to trace inertial motion and tackle bias misalignment errors in (Vasconcelos et al., 2005).

Full state, complex aircraft dynamics have been adopted to enhance the observability of the navigation system in recent work presented in (Bryson and Sukkarieh, 2004; Koifman and Bar-Itzhack, 1999), and experimental results for a model-aided inertial navigation system for underwater vehicles can be found in (Hegrenaes et al., 2008). The navigation system structure is composed by a VD block that plays the role of an extra INS unit. The vehicle dynamics are computed by a vehicle model simulator and the output is compared to the INS state estimates. The EKF state model is augmented to dynamically estimate both the INS and the VD errors, improving the overall navigation system accuracy.

A discussion about the impact of process model complexity on the improvement of the navigation system performance is presented in (Julier and Durrant-Whyte, 2003). Simple vehicle models are shown to tackle state uncertainty and it is evidenced that small improvements in the VD model are more relevant to the performance enhancement than the choice of aiding sensor suites. A drawback in more complex dynamics lies in the modeling errors, over-parametrization of the model, and poor observability of the vehicle states, which bias and degrade the filter performance, and that must be compensated in the form of state model uncertainty and/or using weak constraints. Although very complex models may contain unobservable modes, from the navigation system viewpoint it may only be necessary that a valid combination of the states is observable (Koifman and Bar-Itzhack, 1999).

The proposed navigation system architecture is presented in Fig. 1. The framework is composed by an INS/EKF architecture. The INS is a multirate, high precision algorithm that computes attitude, velocity and position using the data from the inertial sensors. These sensors readings are affected by non-ideal errors, such as bias and noise, that degrade the INS estimates. The EKF compares the aiding sensor and vehicle model information with the INS output, under the form of a measurement residual, and compensates for the estimated inertial unit errors using a direct feedback configuration.

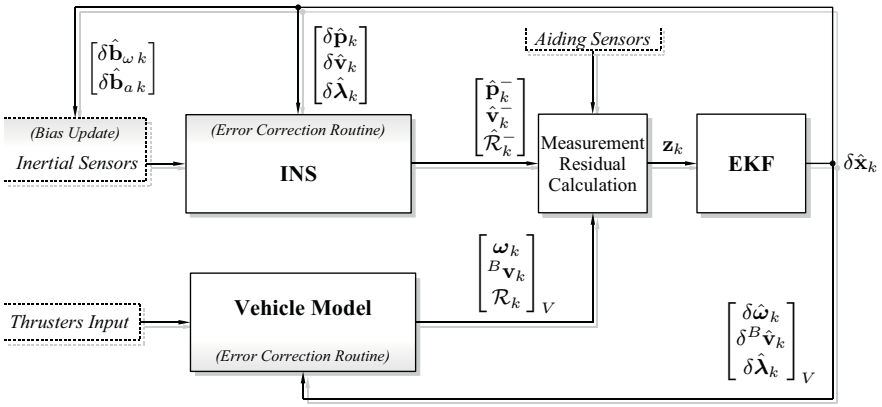

(a) External Vehicle Dynamics

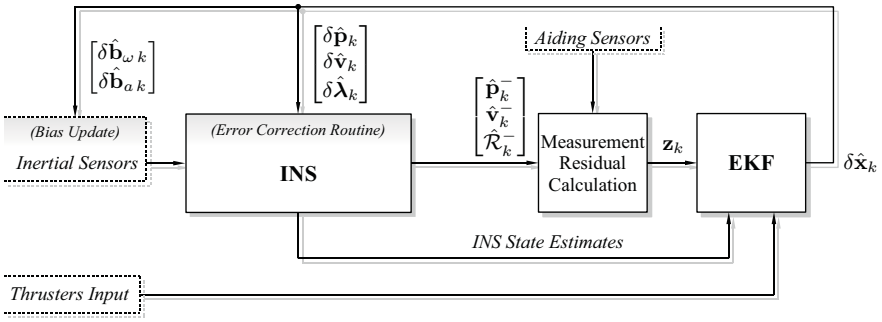

(b) Internal Vehicle Dynamics

Figure 1: Navigation system block diagram

In the first architecture, shown in Fig. 1(a), the vehicle dynamics are computed by an external VD simulator based on the available thrusters input information. The distinct nature of the error sources and system dynamics allows the EKF to separate the INS errors from the VD errors and to perform their mutual updating in the compensation routines. Recalling the fundamentals of filtering and sensor fusion, the VD and INS ensemble is expected to yield better performance than any of the systems independently (Koifman and Bar-Itzhack, 1999). The accuracy of the INS is increased at the cost of integrating the VD model and states, augmenting the EKF states to compensate for the VD model errors, and using error compensation routines in the external vehicle model.

In the second architecture, that is the main contribution of the present paper, the VD information is merged in the EKF state model, as depicted in Fig. 1(b), using the INS states to compute the VD dynamics. In this setup, the inertial state estimates are integrated by both the INS and the VD equations over a sampling interval, and the VD algorithm output are described as a function of the INS errors. The distinct VD and INS integration methods applied to the same inertial quantity enables the EKF to estimate and compensate for the inertial errors.

The proposed technique reduces some of the computations associated with the classical VD aiding, and introduces some flexibility in the implementation of the vehicle model. The use of correction routines in the vehicle simulator is not necessary, due to the embedding of the vehicle dynamics in the filter state model. Because the INS states are used in the VD computations, vehicle model differential equations are partially decoupled and it is possible to select only those dynamics that are more exact. Namely, the attitude kinematics, computed both in the INS and vehicle simulator in the classical aiding technique (Koifman and Bar-Itzhack, 1999), are computed only in the INS in the proposed aiding technique.

The derived vehicle aiding techniques are introduced and validated using a generic fully actuated rigid body simulator for the sake of illustration, and extended to a model-scale Vario X-Treme helicopter model simulator, to demonstrate its application to realistic setups. A preliminary version of this work has been presented in (Vasconcelos et al., 2006), and the application of the proposed architecture for oceanic vehicles has been suggested in (Morgado et al., 2007).

This paper is organized as follows. Section 2 describes the inertial navigation system and the Kalman filtering algorithms adopted in this work. Section 3 presents the vehicle model aiding architectures. Two alternative methods to introduce the vehicle information in the navigation system are detailed. The dynamics of a fully actuated rigid body are described to illustrate the integration of the VD aiding techniques. Section 4 characterizes the LASER sensor and describes the integration of the sensor information in the navigation system structure. Section 5 provides the implementation details. Namely, the state model of the EKF for each aiding technique, the discretization process and the error correction routines are detailed. Simulation results for the VD model and LASER range finder sensor are presented in Section 6. The classical VD is validated using a standard UAV trajectory, and tested with the Vario X-Treme helicopter model. The LASER aiding is demonstrated by simulating a landing maneuver where the distance to ground is unknown. Concluding remarks are discussed in Section 7.

Nomenclature

Column vectors and matrices are denoted respectively by lowercase and uppercase boldface type, e.g. $\mathbf{s}$ and $\mathbf{S}$. The transpose of a vector or matrix will be indicated by a prime, and trailing subscripts $\{x, y, z\}$ denote the vector components, $\mathbf{s} = [s_x \ s_y \ s_z]'$. Leading subscripts and superscripts identify the coordinate system of a quantity, e.g. ${}^{E}\mathbf{s}$ is represented in coordinate frame $\{E\}$, and ${}^{E}_{B}\mathbf{R}$ is a rotation matrix that transforms the vector representation ${}^{B}\mathbf{s}$ into ${}^{E}\mathbf{s}$ by means of the linear operation ${}^{E}\mathbf{s} = {}^{E}_{B}\mathbf{R}\,{}^{B}\mathbf{s}$. Position, velocity and acceleration are denoted respectively by $\mathbf{p}$, $\mathbf{v}$, and $\mathbf{a}$, and the angular velocity of the vehicle expressed in body coordinates is represented by $\boldsymbol{\omega}$. The measurement and the estimate of quantity $\mathbf{s}$ are denoted by $\mathbf{s}_r$ and $\hat{\mathbf{s}}$, respectively. The estimation error is defined as $\delta\mathbf{s} = \hat{\mathbf{s}} - \mathbf{s}$ unless otherwise noted, and $\|\mathbf{s}\|$ denotes the Frobenius norm. Discrete time quantities are characterized by the time index k subscript.

The $(n \times n)$ identity matrix is denoted by $\mathbf{I}_n$, and $(m \times n)$ zeros and ones matrices are respectively denoted by $\mathbf{0}_{m\times n}$ and $\mathbf{1}_{m\times n}$, where the subscript is omitted whenever clear from the context.

2. Navigation System Structure

This section describes the adopted navigation system architecture, that comprises an high-accuracy, multirate INS integration algorithm, combined with advanced error compensation techniques based on the Kalman filtering, as illustrated in Fig. 1. The INS algorithm solves the kinematics differential equations using the output of inertial sensors, which allows for the use of INS in any robotic platform regardless of the available position and attitude references, and irrespective of the vehicle dynamics. However, the INS position and attitude estimation errors will drift with time under the influence of accelerometer and rate gyro non-idealities such as noise, scaling factors, sensor misalignment and bias calibration errors, among others.

The EKF dynamically estimates the INS errors, by merging available aiding information such as GPS position measurements, attitude information contained in vector observations, and vehicle model dynamics, as illustrated in Fig. 1. The INS errors are compensated by modeling the first order description of the INS errors in state space form, comparing the aiding information with the INS estimates, and feeding back the errors estimate to the INS (direct-feedback configuration).

This section presents the main characteristics of the INS and EKF algorithms adopted in this work. The concept of multirate high accuracy inertial integration algorithm, the EKF state space formulation and the error compensation routines are introduced. The navigation system is presented concisely and for the sake of completeness, providing the necessary background for the LASER and the vehicle model aiding techniques, for further details on the present architecture see (Vasconcelos et al., 2005) and references therein.

2.1. Inertial Navigation System

The INS performs attitude, velocity and position numerical integration from rate gyro and accelerometer triads data, rigidly mounted on the vehicle structure (strapdown configuration). For highly maneuverable vehicles, the INS numerical integration must properly address the fast dynamics of inertial sensors output, to avoid estimation errors buildup. The INS algorithm adopted in this paper is found detailed on the tutorial work presented in (Savage, 1998a,b). Angular position, linear velocity, and linear position high frequency motions, referred to as coning, sculling, and scrolling respectively, are properly accounted for using a multirate, recursive approach. In this framework, a high speed, low order algorithm computes dynamic angular rate/acceleration effects at a small sampling interval, and its output is periodically fed to a moderate-speed algorithm that computes attitude/velocity resorting to exact, closed-form equations.

The moderate-speed inertial algorithms attitude output is represented in rotation matrix form, and velocity and position are expressed in Earth frame coordinates. Simulation environments and case study

trajectories to tune the algorithm's execution rates according to performance specifications are described in (Savage, 1998a,b). A standard low-power consumption DSP based hardware architecture is found sufficient to run the algorithm at the highest accuracy repetition rates. Therefore, for a low cost architecture, high computational precision is obtained and the discrete-time integration errors are very small with respect to the other INS error sources such as inertial sensor bias and noise.

2.2. Extended Kalman Filter

The inertial estimation errors are compensated for by merging the INS estimates with aiding information in the EKF algorithm (Brown and Hwang, 1997). The EKF error equations, based on perturbational rigid body kinematics, were brought to full detail in (Britting, 1971), and yield a first-order model of the INS estimation errors and sensor non-idealities. The nominal rigid body kinematics are given by

$$\dot{\mathbf{p}} = \mathbf{v}, \qquad \dot{\mathbf{v}} = \mathcal{R}\,{}^{B}\mathbf{a}, \qquad \dot{\mathcal{R}} = \mathcal{R}\,(\boldsymbol{\omega})_{\times}\,, \tag{1}$$

where $\mathcal{R}$ is the shorthand notation for ${}^{E}_{B}\mathbf{R}$, the Earth and body frames are respectively denoted by $\{E\}$ and $\{B\}$, and $(\mathbf{s})_{\times}$ represents the skew symmetric matrix defined by the vector $\mathbf{s} \in \mathbb{R}^3$ such that $(\mathbf{s})_{\times}\,\mathbf{r} = \mathbf{s} \times \mathbf{r}$, $\mathbf{r} \in \mathbb{R}^3$. The angular velocity and the acceleration of the body are measured respectively by the accelerometer and rate gyro triads, corrupted by noise and bias as follows

$$\boldsymbol{\omega}_r = \boldsymbol{\omega} + \mathbf{b}_\omega + \mathbf{n}_\omega - \hat{\mathbf{b}}_\omega, \tag{2}$$

$$\mathbf{a}_r = {}^{B}\mathbf{a} - {}^{B}\mathbf{g} + \mathbf{b}_a + \mathbf{n}_a - \hat{\mathbf{b}}_a, \tag{3}$$

where $\mathbf{g}$ represents Earth's gravitational field, the sensor biases are denoted by $\mathbf{b}_a$ and $\mathbf{b}_\omega$, and $\mathbf{n}_a \sim \mathcal{N}(\mathbf{0}, \Xi_a)$, $\mathbf{n}_\omega \sim \mathcal{N}(\mathbf{0}, \Xi_\omega)$ are Gaussian white noises. The inertial sensor biases are modeled as random walk processes,

$$\dot{\mathbf{b}}_a = \mathbf{n}_{b_a}, \quad \dot{\mathbf{b}}_\omega = \mathbf{n}_{b_\omega},$$

where $\mathbf{n}_{b_a} \sim \mathcal{N}(\mathbf{0}, \Xi_{b_a})$, $\mathbf{n}_{b_\omega} \sim \mathcal{N}(\mathbf{0}, \Xi_{b_\omega})$ are Gaussian white noises.

The rigid body coordinates are estimated using the available inertial sensor information

$$\dot{\hat{\mathbf{p}}} = \hat{\mathbf{v}}, \qquad \dot{\hat{\mathbf{v}}} = \hat{\mathcal{R}}\mathbf{a}_r + {}^{E}\mathbf{g}, \qquad \dot{\hat{\mathcal{R}}} = \hat{\mathcal{R}}\,(\boldsymbol{\omega}_r)_{\times}\,, \qquad \dot{\hat{\mathbf{b}}}_a = \mathbf{0}, \qquad \dot{\hat{\mathbf{b}}}_\omega = \mathbf{0}. \tag{4}$$

The position, velocity and bias estimation errors are defined by the difference of the estimated and nominal quantities,

$$\delta\mathbf{p} := \hat{\mathbf{p}} - \mathbf{p}, \qquad \delta\mathbf{v} := \hat{\mathbf{v}} - \mathbf{v}, \qquad \delta\mathbf{b}_a := \hat{\mathbf{b}}_a - \mathbf{b}_a, \qquad \delta\mathbf{b}_\omega := \hat{\mathbf{b}}_\omega - \mathbf{b}_\omega,$$

and the attitude error, denoted as $\delta\boldsymbol{\lambda}$, is parametrized by an unconstrained rotation vector representation in Earth coordinates, which can be assumed locally linear and non-singular, for details and equivalent attitude

parametrizations, see (Markley, 2003; Pittelkau, 2003). Define the rotation error matrix as $\mathbf{R}(\delta\boldsymbol{\lambda}) := \hat{\mathcal{R}}\mathcal{R}'$, the attitude error rotation vector $\delta\boldsymbol{\lambda}$ is described by the first order approximation

$$\mathbf{R}(\delta\boldsymbol{\lambda}) \simeq \mathbf{I}_3 + (\delta\boldsymbol{\lambda})_\times \Rightarrow (\delta\boldsymbol{\lambda})_\times \simeq \hat{\mathcal{R}}\mathcal{R}' - \mathbf{I}_3, \tag{5}$$

that is valid for "small-angle" attitude errors (Britting, 1971).

Combining (1-4), the attitude, velocity, and position error kinematics are obtained by retaining the first-order terms of Taylor's series expansions or by using perturbation algebraic techniques (Britting, 1971), producing

$$\delta\dot{\mathbf{p}} = \delta\mathbf{v}, \quad \delta\dot{\mathbf{v}} = \hat{\mathcal{R}}(\mathbf{a}_r - \mathbf{a}_{\mathrm{SF}}) - \left(\hat{\mathcal{R}}\mathbf{a}_r\right)_\times \delta\boldsymbol{\lambda}, \quad \delta\dot{\boldsymbol{\lambda}} = \mathcal{R}(\boldsymbol{\omega}_r - \boldsymbol{\omega}),$$
$$\delta\dot{\mathbf{b}}_a = -\mathbf{n}_{b_a}, \quad \delta\dot{\mathbf{b}}_\omega = -\mathbf{n}_{b_\omega}, \tag{6}$$

where $\mathbf{a}_{\mathrm{SF}} = {}^B\mathbf{a} - {}^B\mathbf{g}$ is the specific force, defined as the nominal reading of an accelerometer. The terms $(\boldsymbol{\omega}_r - \boldsymbol{\omega})$ and $(\mathbf{a}_r - \mathbf{a}_{\mathrm{SF}})$ represent the non-idealities of the accelerometer and rate gyro readings (2) and (3) respectively, and are described by

$$(\boldsymbol{\omega}_r - \boldsymbol{\omega}) = -\delta\mathbf{b}_\omega + \mathbf{n}_\omega, \qquad (\mathbf{a}_r - \mathbf{a}_{\mathrm{SF}}) = -\delta\mathbf{b}_a + \mathbf{n}_a. \tag{7}$$

Combining (6) and (7), the error state space model is

$$\delta\dot{\mathbf{p}} = \delta\mathbf{v}, \qquad \delta\dot{\mathbf{v}} = -\hat{\mathcal{R}}\delta\mathbf{b}_a - \left(\hat{\mathcal{R}}\mathbf{a}_r\right)_\times \delta\boldsymbol{\lambda} + \hat{\mathcal{R}}\mathbf{n}_a, \qquad \delta\dot{\boldsymbol{\lambda}} = -\hat{\mathcal{R}}\delta\mathbf{b}_\omega + \hat{\mathcal{R}}\mathbf{n}_\omega,$$
$$\delta\dot{\mathbf{b}}_a = -\mathbf{n}_{b_a}, \qquad \delta\dot{\mathbf{b}}_\omega = -\mathbf{n}_{b_\omega}. \tag{8}$$

The Kalman filter adopted in this work is based on the concept of Multiplicative EKF. The adopted attitude error parametrization is locally linear and hence can be integrated in the EKF estimation algorithm without violating constraints such as those found in rotation matrices and quaternions. The EKF estimates the INS error vector $\delta\mathbf{x} = \begin{bmatrix}\delta\mathbf{p}' & \delta\mathbf{v}' & \delta\boldsymbol{\lambda}' & \delta\mathbf{b}_a' & \delta\mathbf{b}_\omega'\end{bmatrix}'$ based on the aiding information. To preserves the small error assumption underlying the linearized model (8), $\delta\mathbf{x}$ is fed back and stored in the global quantity $\mathbf{x}_{\mathrm{INS}} = (\mathbf{p}, \mathbf{v}, \mathcal{R}, \mathbf{b}_a, \mathbf{b}_\omega)$ of the INS, and reset in the filter, as illustrated in Fig. 1. The validity of this process is demonstrated in (Markley, 2003), where it is also evidenced that the estimation error covariance is unaffected when $\delta\mathbf{x}$ is incorporated in $\mathbf{x}_{\mathrm{INS}}$.

3. Vehicle Model Aiding

Classical GPS/INS architectures that compensate for inertial sensor biases are found to hold only partial observability for time-invariant configurations (Goshen-Meskin and Bar-Itzhack, 1992a,b). The vehicle model aiding steps forward as an inexpensive, software based solution to overcome the lack of observability in the navigation system. Given the vehicle model inputs, the vehicle dynamics provide angular and

linear velocities information, that can be merged with the INS estimates using the EKF algorithm. Observability of the inertial states is enhanced and although position is in general unobservable from the vehicle dynamics (Bryson and Sukkarieh, 2004), the velocity accuracy improvements will reduce the drift of the position estimation errors, as shown in the results presented in the literature (Hegrenaes et al., 2008; Bar-Itzhack and Harman, 2003; Bryson and Sukkarieh, 2004).

This section presents the VD model and the architecture to integrate the VD information in the navigation system, depicted in Fig. 1, is introduced and detailed. In particular, a new methodology to directly embed the vehicle information in the EKF is presented.

The external VD structure, depicted in Fig. 1(a), follows from previous work found in (Koifman and Bar-Itzhack, 1999; Bryson and Sukkarieh, 2004), where the integration of the VD in the system is analogous to that adopted for the INS. Vehicle state estimates are computed by a vehicle simulator block, using the thrusters input information. The full state vehicle model algorithm computes attitude and velocity estimates that are compared to the INS output, under the form of measurement residuals. Whereas the vehicle aiding information is expected to help the INS, computational and modeling errors of the vehicle dynamics itself must be addressed by the filter. Therefore, the EKF state model is also augmented to compensate for the vehicle modeling errors.

The current work presents an alternative method to exploit the VD model by blending the vehicle simulator equations directly in the EKF state model. Vehicle dynamics are integrated in the filter state space, linearized about the inertial state estimates. The vehicle dynamics propagate the inertial estimates, so the VD integration is a function of the INS errors. Therefore, the EKF algorithm internally solves the VD equations and only outputs the INS error estimates, as shown in Fig. 1(b).

Without any loss of generality, the VD aiding technique proposed in this paper is illustrated using the dynamics of a 6-DOF rigid body polyhedron with uniform mass density and fully actuated. The Vario X-Treme helicopter dynamic model, detailed in Appendix A, is highly nonlinear and coupled, and is addressed later to evidence that the VD aiding technique is valid for realistic robotic platforms.

3.1. Rigid Body Dynamics

The body coordinate frame origin, denoted $\mathbf{p}_{Borg}$, is located at the body's center of mass and geometric center. The axes of the body frame define a plane of symmetry for the mass distribution of the body, so the resulting body inertia tensor, denoted $\mathbf{I}_B$, is described by the principal moments of inertia (Craig, 1989), yielding

$$\mathbf{I}_B = \frac{m}{12}\begin{bmatrix} h^2+l^2 & 0 & 0 \\ 0 & w^2+h^2 & 0 \\ 0 & 0 & l^2+w^2 \end{bmatrix},$$

where m is the body mass and (l, w, h) represent the polyhedron length, width and height, respectively. The rigid body is subject to the thrusters force and momentum, denoted by $\mathbf{f}_{\text{th}}$ and $\mathbf{n}_{\text{th}}$ respectively, and to viscous linear and angular damping, denoted by $\mathbf{f}_d$ and $\mathbf{n}_d$ respectively, yielding

$$^B\mathbf{f}_{\text{th}} = \sum_i {}^B\mathbf{f}_i, \qquad {}^B\mathbf{n}_{\text{th}} = \sum_i {}^B\mathbf{p}_{\text{th}\,i} \times {}^B\mathbf{f}_i, \qquad {}^B\mathbf{f}_d = -K_{\text{lin}}\,{}^B\mathbf{v}, \qquad {}^B\mathbf{n}_d = -K_{\text{ang}}\boldsymbol{\omega},$$

where $i = 1, \ldots, 6$ is the index of the thruster applying force $\mathbf{f}_i$ to the body, ${}^B\mathbf{p}_{\text{th}\,i}$ are the thrusters' coordinates in body frame, and K_{lin} and K_{ang} are respectively the linear and the angular damping coefficients.

Applying the Newton and Euler equations to determine body's translation and rotation with respect to the inertial frame, the body dynamics are expressed by the nonlinear state space model

$$\dot{\boldsymbol{\omega}}_V := f_\omega(\boldsymbol{\omega}_V, \mathbf{n}_{\text{th}}) = -\mathbf{I}_B^{-1}\left((\boldsymbol{\omega}_V)_\times \mathbf{I}_B\boldsymbol{\omega}_V + K_{\text{ang}}\boldsymbol{\omega}_V\right) + \mathbf{I}_B^{-1}\mathbf{n}_{\text{th}}, \tag{9a}$$

$${}^B\dot{\mathbf{v}}_V := f_v(\boldsymbol{\omega}_V, {}^B\mathbf{v}_V, \mathbf{f}_{\text{th}}) = -\mathbf{M}_T^{-1}\left((\boldsymbol{\omega}_V)_\times \mathbf{M}_T\,{}^B\mathbf{v}_V + K_{\text{lin}}\,{}^B\mathbf{v}_V\right) + \mathbf{M}_T^{-1}\mathbf{f}_{\text{th}} + \mathcal{R}'_V\,{}^E\mathbf{g}, \tag{9b}$$

$$\dot{\mathcal{R}}_V := f_{\mathcal{R}}(\boldsymbol{\omega}_V, \mathcal{R}_V) = \mathcal{R}_V\,(\boldsymbol{\omega}_V)_\times\,, \tag{9c}$$

where the body and center of mass coordinate frames are defined with the same orientation and position, so that the body frame attitude dynamics (9a) do not depend on the linear velocity. To avoid ambiguity in the adopted notation, ${}^B\dot{\mathbf{v}}$ denotes $\frac{\mathrm{d}\,{}^B\mathbf{v}}{\mathrm{dt}}$, whereas ${}^B(\frac{\mathrm{d}\,\mathbf{v}}{\mathrm{dt}})$ is denoted by ${}^B(\dot{\mathbf{v}})$.

The simple rigid body dynamics (9) allow for physical intuition on the contribution of the vehicle model to the inertial states errors compensation. The V subscript for the angular velocity and body linear velocity (9) is adopted to emphasize that these quantities are computed using the vehicle dynamics, given that some are also computed by the INS, using distinct integration algorithms and inputs.

3.2. External Vehicle Model Aiding

In the classical VD aiding, presented in Fig. 1(a), the vehicle dynamics are computed using a standalone vehicle simulator, included in the navigation system but external to the EKF/INS system. The EKF state model is augmented to estimate and compensate for the VD block errors, using model specific error compensation routines.

The VD block error dynamics are formulated using the technique adopted to describe the INS error dynamics in Section 2.2. These are obtained by applying a perturbational analysis to the nominal dynamics (9). Let $\hat{\mathbf{x}}_V = (\hat{\boldsymbol{\omega}}_V, {}^B\hat{\mathbf{v}}_V, \hat{\mathcal{R}}_V)$ denote the states estimated by the vehicle model simulator, the vehicle model

error dynamics are described by the first order terms of the Taylor series expansion

$$\dot{\hat{\boldsymbol{\omega}}}_V = f_\omega(\hat{\boldsymbol{\omega}}_V, \hat{\mathbf{n}}_{\text{th}}) \Rightarrow \dot{\delta\boldsymbol{\omega}}_V \approx \left.\frac{\partial f_\omega}{\partial \boldsymbol{\omega}}\right|_{\mathbf{x}_V} \delta\boldsymbol{\omega}_V + \left.\frac{\partial f_\omega}{\partial \mathbf{n}_{\text{th}}}\right|_{\mathbf{x}_V} \delta\mathbf{n}_{\text{th}}, \tag{10a}$$

$$\begin{aligned} {}^B\dot{\hat{\mathbf{v}}}_V &= f_v(\hat{\boldsymbol{\omega}}_V, {}^B\hat{\mathbf{v}}_V, \hat{\mathcal{R}}_V, \hat{\mathbf{f}}_{\text{th}}) \Rightarrow \\ \dot{\delta^B\mathbf{v}}_V &\approx \left.\frac{\partial f_v}{\partial \boldsymbol{\omega}_V}\right|_{\mathbf{x}_V} \delta\boldsymbol{\omega}_V + \left.\frac{\partial f_v}{\partial {}^B\mathbf{v}_V}\right|_{\mathbf{x}_V} \delta^B\mathbf{v}_V + \left.\frac{\partial f_v}{\partial \delta\boldsymbol{\lambda}}\right|_{\mathbf{x}_V} \delta\boldsymbol{\lambda}_V + \left.\frac{\partial f_v}{\partial \mathbf{f}_{\text{th}}}\right|_{\mathbf{x}_V} \delta\mathbf{f}_{\text{th}}, \end{aligned} \tag{10b}$$

$$\dot{\hat{\mathcal{R}}}_V = f_{\mathcal{R}}(\hat{\boldsymbol{\omega}}_V, \hat{\mathcal{R}}_V) \Rightarrow \dot{\delta\boldsymbol{\lambda}}_V = \mathcal{R}_V \delta\boldsymbol{\omega}_V, \tag{10c}$$

where $\delta\boldsymbol{\omega}_V = \hat{\boldsymbol{\omega}}_V - \boldsymbol{\omega}$, $\delta^B\mathbf{v}_V = {}^B\hat{\mathbf{v}}_V - {}^B\mathbf{v}$, $\delta\mathbf{n}_{\text{th}} = \hat{\mathbf{n}}_{\text{th}} - \mathbf{n}_{\text{th}}$, $\delta\mathbf{f}_{\text{th}} = \hat{\mathbf{f}}_{\text{th}} - \mathbf{f}_{\text{th}}$, and the Jacobians are given by

$$\begin{aligned} \left.\frac{\partial f_\omega}{\partial \boldsymbol{\omega}}\right|_{\mathbf{x}_V} &= \mathbf{I}_B^{-1}\left((\mathbf{I}_B\boldsymbol{\omega}_V)_\times - (\boldsymbol{\omega}_V)_\times \mathbf{I}_B - \mathbf{I}_3\, K_{\text{ang}}\right), & \left.\frac{\partial f_\omega}{\partial \mathbf{n}_{\text{th}}}\right|_{\mathbf{x}_V} &= \mathbf{I}_B^{-1}, \\ \left.\frac{\partial f_v}{\partial \boldsymbol{\omega}}\right|_{\mathbf{x}_V} &= \mathbf{M}_T^{-1}\left(\mathbf{M}_T\, {}^B\mathbf{v}_V\right)_\times, & \left.\frac{\partial f_v}{\partial \mathbf{f}_{\text{th}}}\right|_{\mathbf{x}_V} &= \mathbf{M}_T^{-1}, \\ \left.\frac{\partial f_v}{\partial {}^B\mathbf{v}}\right|_{\mathbf{x}_V} &= \mathbf{M}_T^{-1}\left(-(\boldsymbol{\omega}_V)_\times \mathbf{M}_T - \mathbf{I}_3\, K_{\text{lin}}\right), & \left.\frac{\partial f_v}{\partial \delta\boldsymbol{\lambda}}\right|_{\mathbf{x}_V} &= \mathcal{R}'_V\left({}^E\mathbf{g}\right)_\times, \end{aligned} \tag{11}$$

The first order model (10) can also be obtained by perturbational analysis of the dynamics (9). The rotation matrix dynamics (9c) are identical to the inertial rigid body kinematics expressed in (1), and consequently do not yield new information to the system. However, the computation of $\mathcal{R}_V$ is necessary for the vehicle dynamics simulator (9), and the associated error dynamics (10c), which are identical to the INS attitude error (6), must be compensated for.

The INS and VD state estimates are compared under the form of measurement residuals, obtained by the perturbational method (Britting, 1971), and described by

$$\mathbf{z}_\omega := \hat{\boldsymbol{\omega}} - \hat{\boldsymbol{\omega}}_V = \boldsymbol{\omega} + \delta\boldsymbol{\omega} - (\boldsymbol{\omega} + \delta\boldsymbol{\omega}_V) = \delta\boldsymbol{\omega} - \delta\boldsymbol{\omega}_V = -\delta\mathbf{b}_\omega - \delta\boldsymbol{\omega}_V + \mathbf{n}_\omega, \tag{12a}$$

$$\begin{aligned} \mathbf{z}_u &:= \hat{\mathcal{R}}'\hat{\mathbf{v}} - {}^B\hat{\mathbf{v}}_V = \hat{\mathcal{R}}'\mathbf{v} - ({}^B\mathbf{v} + \delta^B\mathbf{v}_V) = (\hat{\mathcal{R}}' - \mathcal{R}')\mathbf{v} + \mathcal{R}'\delta\mathbf{v} - \delta^B\mathbf{v}_V \\ &= -\hat{\mathcal{R}}'\left(\boldsymbol{\lambda}\right)_\times \mathbf{v} + \mathcal{R}'\delta\mathbf{v} - \delta^B\mathbf{v}_V \approx \mathcal{R}'\delta\mathbf{v} + \mathcal{R}'\left(\mathbf{v}\right)_\times \delta\boldsymbol{\lambda} - \delta^B\mathbf{v}_V, \end{aligned} \tag{12b}$$

$$\mathbf{z}_{\mathcal{R}} := \hat{\mathcal{R}}\hat{\mathcal{R}}'_V - \mathbf{I} \approx \left[\mathbf{I} + (\delta\boldsymbol{\lambda})_\times\right]\mathcal{R}\mathcal{R}'\left[\mathbf{I} - (\delta\boldsymbol{\lambda}_V)_\times\right] - \mathbf{I} \approx \delta\boldsymbol{\lambda} - \delta\boldsymbol{\lambda}_V. \tag{12c}$$

The vehicle model equations (9) are computed by a variable-step Runge-Kutta differential equation solver, using the thrusters force $\mathbf{f}_{\text{th}}$ and momentum $\mathbf{n}_{\text{th}}$ information. The vehicle state errors and covariances are propagated by the EKF using the first order model (10) and assuming that the thrusters input is known from the control system, $\delta\mathbf{n}_{\text{th}} = \delta\mathbf{f}_{\text{th}} = \mathbf{0}$. In experimental applications the inputs of the vehicle model may not be accurately known, and $\delta\mathbf{n}_{\text{th}}$, $\delta\mathbf{f}_{\text{th}}$ may be modeled as small stochastic uncertainties to increase the navigation system robustness.

The INS and VD errors are estimated by processing the measurement residuals (12) in the EKF algorithm. Similar to the storage technique used for the INS error compensation, described in Section 2.2, the estimated VD errors $\delta\mathbf{x}_V = \begin{bmatrix}\delta\boldsymbol{\omega}'_V & \delta^B\mathbf{v}'_V & \delta\boldsymbol{\lambda}'_V\end{bmatrix}'$ are transferred to the external VD block and used to update the

state $\mathbf{x}_V = (\boldsymbol{\omega}_V, {}^B\mathbf{v}_V, \mathcal{R}_V)$. This method preserves the small error conditions of the first order model (9), however it requires the implementation of error compensation routines in the vehicle model.

3.3. Internal Vehicle Model Aiding

The vehicle model aiding enhances the accuracy of the navigation system by providing specific information about the robotic platform, e.g. its linear and angular velocity dynamics, (9a) and (9b) respectively. In the classical technique described in the last section, the attitude kinematics (9c) are computed simultaneously in the INS and in the self-contained vehicle simulator, and vehicle model errors compensation routines must be implemented, as illustrated in Fig. 1. The necessity of these auxiliary computational routines motivates an alternative vehicle model integration method.

The embedded VD aiding concept is based on combining vehicle states such as $\boldsymbol{\omega}_V$, ${}^B\mathbf{v}_V$ and $\mathcal{R}_V$, with the corresponding INS estimates, respectively $\hat{\boldsymbol{\omega}}$, $\hat{\mathcal{R}}'\hat{\mathbf{v}}$ and $\hat{\mathcal{R}}$, by propagating the inertial quantities using the vehicle dynamics. The VD results are described as a function of the INS errors, enabling the EKF to estimate and compensate for the inertial errors. Consequently, error estimation and compensation routines are only performed in the INS, reducing the computational cost associated to VD aiding techniques.

With a slight abuse of notation, let $\hat{\mathbf{x}} = (\hat{\boldsymbol{\omega}}, \hat{\mathbf{v}}, \hat{\mathcal{R}}, \hat{\mathbf{b}}_a, \hat{\mathbf{b}}_\omega)$ denote the INS state estimates. In the internal VD methodology, nominal vehicle dynamics (9) are linearized about the INS state estimates. Using the first order terms of the Taylor series expansion yields

$$
\begin{aligned}
\dot{\boldsymbol{\omega}} =& f_\omega(\boldsymbol{\omega}, \mathbf{n}_{\text{th}}) \approx f_\omega(\hat{\boldsymbol{\omega}}, \hat{\mathbf{n}}_{\text{th}}) + \left.\frac{\partial f_\omega}{\partial \boldsymbol{\omega}}\right|_{\hat{\mathbf{x}}} (\boldsymbol{\omega} - \hat{\boldsymbol{\omega}}) + \left.\frac{\partial f_\omega}{\partial \mathbf{n}_{\text{th}}}\right|_{\hat{\mathbf{x}}} (\mathbf{n}_{\text{th}} - \hat{\mathbf{n}}_{\text{th}}),\\
{}^B\dot{\mathbf{v}} =& f_v(\boldsymbol{\omega}, {}^B\mathbf{v}, \mathcal{R}, \mathbf{f}_{\text{th}}) \approx f_v(\hat{\boldsymbol{\omega}}, {}^B\hat{\mathbf{v}}, \hat{\mathcal{R}}, \hat{\mathbf{f}}_{\text{th}}) + \left.\frac{\partial f_v}{\partial \boldsymbol{\omega}}\right|_{\hat{\mathbf{x}}} (\boldsymbol{\omega} - \hat{\boldsymbol{\omega}})\\
&+ \left.\frac{\partial f_v}{\partial {}^B\mathbf{v}}\right|_{\hat{\mathbf{x}}} ({}^B\mathbf{v} - {}^B\hat{\mathbf{v}}) + \left.\frac{\partial f_v}{\partial \delta\boldsymbol{\lambda}}\right|_{\hat{\mathbf{x}}} \delta\boldsymbol{\lambda} + \left.\frac{\partial f_v}{\partial \mathbf{f}_{\text{th}}}\right|_{\hat{\mathbf{x}}} (\mathbf{f}_{\text{th}} - \hat{\mathbf{f}}_{\text{th}}).
\end{aligned}
$$

The INS estimate error is defined as the difference between the nominal state and the INS estimate. Therefore, the nominal angular and linear velocities are expressed as a function of the INS states and estimation errors by

$$
\begin{aligned}
\dot{\boldsymbol{\omega}} &\approx f_\omega(\hat{\boldsymbol{\omega}}, \hat{\mathbf{n}}_{\text{th}}) - \left.\frac{\partial f_\omega}{\partial \boldsymbol{\omega}}\right|_{\hat{\mathbf{x}}} \delta\boldsymbol{\omega} - \left.\frac{\partial f_\omega}{\partial \mathbf{n}_{\text{th}}}\right|_{\hat{\mathbf{x}}} \delta\mathbf{n}_{\text{th}}\\
&= f_\omega(\hat{\boldsymbol{\omega}}, \hat{\mathbf{n}}_{\text{th}}) + \left.\frac{\partial f_\omega}{\partial \boldsymbol{\omega}}\right|_{\hat{\mathbf{x}}} \delta\mathbf{b}_\omega - \left.\frac{\partial f_\omega}{\partial \boldsymbol{\omega}}\right|_{\hat{\mathbf{x}}} \mathbf{n}_\omega - \left.\frac{\partial f_\omega}{\partial \mathbf{n}_{\text{th}}}\right|_{\hat{\mathbf{x}}} \delta\mathbf{n}_{\text{th}}, \qquad (13a)\\
{}^B\dot{\mathbf{v}} &\approx f_v(\hat{\boldsymbol{\omega}}, {}^B\hat{\mathbf{v}}, \hat{\mathcal{R}}, \hat{\mathbf{f}}_{\text{th}}) - \left.\frac{\partial f_v}{\partial \boldsymbol{\omega}}\right|_{\hat{\mathbf{x}}} \delta\boldsymbol{\omega} - \left.\frac{\partial f_v}{\partial {}^B\mathbf{v}}\right|_{\hat{\mathbf{x}}} \delta{}^B\mathbf{v} - \left.\frac{\partial f_v}{\partial \delta\boldsymbol{\lambda}}\right|_{\hat{\mathbf{x}}} \delta\boldsymbol{\lambda}\\
&\quad - \left.\frac{\partial f_v}{\partial \mathbf{n}_{\text{th}}}\right|_{\hat{\mathbf{x}}} \delta\mathbf{n}_{\text{th}} - \left.\frac{\partial f_v}{\partial \mathbf{f}_{\text{th}}}\right|_{\hat{\mathbf{x}}} \delta\mathbf{f}_{\text{th}}\\
&= f_v(\hat{\boldsymbol{\omega}}, {}^B\hat{\mathbf{v}}, \hat{\mathcal{R}}, \hat{\mathbf{f}}_{\text{th}}) - \left.\frac{\partial f_v}{\partial {}^B\mathbf{v}}\right|_{\hat{\mathbf{x}}} \mathcal{R}'\delta\mathbf{v} - \left(\left.\frac{\partial f_v}{\partial \delta\boldsymbol{\lambda}}\right|_{\hat{\mathbf{x}}} + \left.\frac{\partial f_v}{\partial \mathbf{v}}\right|_{\hat{\mathbf{x}}} \mathcal{R}' (\mathbf{v})_\times\right) \delta\boldsymbol{\lambda}
\end{aligned}
$$

$$+ \left.\frac{\partial f_v}{\partial \boldsymbol{\omega}}\right|_{\hat{\mathbf{x}}} \delta\mathbf{b}_\omega - \left.\frac{\partial f_v}{\partial \boldsymbol{\omega}}\right|_{\hat{\mathbf{x}}} \mathbf{n}_\omega - \left.\frac{\partial f_v}{\partial \mathbf{n}_{\text{th}}}\right|_{\hat{\mathbf{x}}} \delta\mathbf{n}_{\text{th}} - \left.\frac{\partial f_v}{\partial \mathbf{f}_{\text{th}}}\right|_{\hat{\mathbf{x}}} \delta\mathbf{f}_{\text{th}}, \tag{13b}$$

where body linear velocity error $\delta^B\mathbf{v}$ is rewritten as a function of the INS state errors $\delta^B\mathbf{v} := \hat{\mathcal{R}}'\hat{\mathbf{v}} - \mathcal{R}'\mathbf{v} \approx \mathcal{R}'\left(\mathbf{v}\right)_\times \delta\boldsymbol{\lambda} + \mathcal{R}'\delta\mathbf{v}$.

The first order model (13) describes the nominal angular and linear dynamics as the result of solving the vehicle dynamics $f_\omega(\hat{\boldsymbol{\omega}}, \hat{\mathbf{n}}_{\text{th}})$ and $f_v(\hat{\boldsymbol{\omega}}, {}^B\hat{\mathbf{v}}, \hat{\mathcal{R}}, \hat{\mathbf{f}}_{\text{th}})$ using the INS states. Interestingly enough, the vehicle dynamics functions applied to the inertial estimates do not yield the INS state estimate derivatives, $\dot{\hat{\boldsymbol{\omega}}} \neq f_\omega(\hat{\boldsymbol{\omega}}, \hat{\mathbf{n}}_{\text{th}})$, ${}^B\dot{\hat{\mathbf{v}}} \neq f_v(\hat{\boldsymbol{\omega}}, {}^B\hat{\mathbf{v}}, \hat{\mathcal{R}}, \hat{\mathbf{f}}_{\text{th}})$, which is a clear consequence of the distinct, compatible models enclosed in the VD and INS computations. The error dynamics (13) are a function of the Jacobians computed for the classical method (11), and hence the first order analytical results needed to integrate the vehicle model in the EKF state model are the same for both architectures.

The navigation system observations are drawn directly from the INS inertial estimates

$$\mathbf{z}_\omega := \hat{\boldsymbol{\omega}} = \boldsymbol{\omega} - \delta\mathbf{b}_\omega + \mathbf{n}_\omega, \tag{14a}$$

$$\mathbf{z}_u := \hat{\mathcal{R}}'\hat{\mathbf{v}} = \mathcal{R}'\left(\mathbf{I} - \left(\delta\boldsymbol{\lambda}\right)_\times\right)\mathbf{v} + \mathcal{R}'\delta\mathbf{v} \approx {}^B\mathbf{v} + \mathcal{R}'\delta\mathbf{v} + \mathcal{R}'\left(\mathbf{v}\right)_\times \delta\boldsymbol{\lambda}. \tag{14b}$$

The alternative method allows for the selection of a subset of the vehicle model differential equations, namely the model dynamics that are more accurate and whose parameters are less uncertain. For example, the navigation system can be aided by using VD linear velocity dynamics (9b) without computing the angular velocity dynamics (9a) if these are inaccurate.

While the classical VD technique replicated the attitude kinematics as presented in (10c), the proposed VD aiding technique integrates (9a-9b) using the INS attitude estimate $\hat{\mathcal{R}}$, yielding a smaller number of states in the system and estimates in the filter. This reduces the computational resources required for the integration of vehicle dynamics in the navigation system. Also, error compensation routines for the vehicle model are not necessary in this technique because the vehicle dynamics are integrated in the filter state model.

4. LASER Aiding

In this section, the LASER range finder aiding sensor is described and the corresponding filter observation equation is introduced. The LASER reads the distance L from the vehicle to the ground, along the z axis of the $\{M\}$ coordinate frame, as depicted in Fig. 2. By processing this information in the filter architecture, an estimate of the vehicle's distance to the ground can be obtained with high accuracy, as required for landing and takeoff operations of an air vehicle. Other changeling applications for the LASER sensor are the relative positioning of the vehicle with respect to a structure. Without loss of generality, the sensor is assumed to be mounted along the z axis of the frame $\{M\}$, whose relative orientation to the body frame is described by the

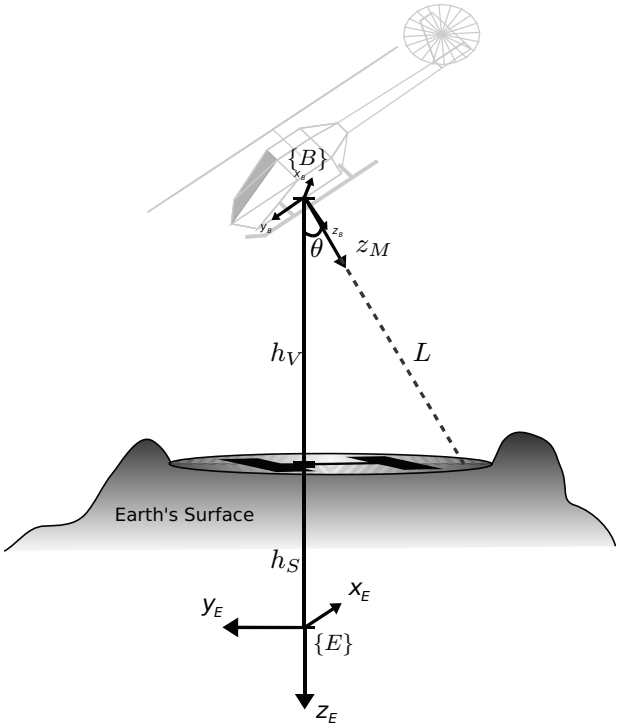

Figure 2: LASER Range Finder Reading

known installation rotation matrix ${}^{B}_{M}\mathbf{R}$, for calibration methods see (Guerreiro et al., 2008) and references therein.

In the current work, the landing area terrain is assumed to be locally planar, such as an heliport or a landing lane. The Earth's surface height h_S, given by the distance from the Earth frame origin to the Earth surface, is modeled as approximately constant

$$\dot{h}_S = n_{h_S}, \tag{15}$$

where $n_{h_S} \sim \mathcal{N}(0, \Xi_{h_S})$ is a Gaussian white noise whose variance reflects the uncertainty on the ground's flatness. As depicted in Fig. 2, the z axis Earth coordinate of the vehicle is given by

$$p_z = -(h_S + h_V), \tag{16}$$

where $h_V \geq 0$ is the vehicle's height, that is, the distance from Body frame origin to the Earth surface.

Using elementary trigonometric relations yields

$$\cos(\theta) = \frac{h_V}{L} = \frac{|{}^{M}\mathbf{h}'_V \mathbf{e}_z|}{|{}^{E}\mathbf{h}'_V \mathbf{e}_z|},$$

where ${}^{E}\mathbf{h}_V = \begin{bmatrix} 0 & 0 & -h_V \end{bmatrix}'$ is the vehicle's height in Earth coordinates, $\mathbf{e}_z = \begin{bmatrix} 0 & 0 & 1 \end{bmatrix}'$ is the unitary z axis vector and ${}^{M}\mathbf{h}'_V \mathbf{e}_z$ corresponds to the projection of $\mathbf{h}_V$ on the z axis of the $\{M\}$ frame. Applying the

coordinate transform ${}^{M}\mathbf{h}_V = {}^{B}_{M}\mathbf{R}'\mathcal{R}'^{E}\mathbf{h}_V$ and developing the terms in the previous equation, the LASER range is described by

$$L = \begin{cases} \frac{h_V}{\mathbf{e}_z'\mathcal{R}\,{}^{B}_{M}\mathbf{R}\mathbf{e}_z}, & \text{if } \mathbf{e}_z'\mathcal{R}\,{}^{B}_{M}\mathbf{R}\mathbf{e}_z > 0 \\ \text{not defined}, & \text{if } \mathbf{e}_z'\mathcal{R}\,{}^{B}_{M}\mathbf{R}\mathbf{e}_z \leq 0 \end{cases}, \tag{17}$$

that is not defined for the cases where the LASER is pointing upwards. The LASER range finder sensor measures the actual range L corrupted by the sensor noise

$$L_r = L + \delta L, \tag{18}$$

where $\delta L = n_L$ is modeled as a zero-mean, Gaussian white noise with variance Ξ_L.

The LASER sensor is used primarily to perform landing maneuvers, providing high accuracy estimates of the vehicle distance to the ground along the $\{M\}$ coordinate frame z axis. The measurement residual is computed by

$$\mathbf{z}_L := \hat{p}_z - \left(-\hat{h}_V\right), \tag{19}$$

where the height estimate from the LASER reading is given by rearranging the terms in (17) and using the INS estimates in the unknown terms, producing

$$\hat{h}_V = \mathbf{e}_z'\hat{\mathcal{R}}\,{}^{B}_{M}\mathbf{R}\mathbf{e}_z L_r. \tag{20}$$

The vehicle's and Earth's surface heights, h_S and h_V respectively, are filtered apart by modeling the h_S dynamics (15) in the EKF, measuring h_V from the LASER reading as in (20), and feeding the measurement residual (19) to the EKF.

To model of the measurement residual (19) in the EKF, the INS position estimate is expressed as a function of the vehicle and Earth's surface heights, given by

$$\hat{p}_z = p_z + \delta p_z = -h_S - h_V + \mathbf{e}_z'\delta\mathbf{p}. \tag{21}$$

Expanding the INS attitude estimate $\hat{\mathcal{R}}$ with the attitude error $\delta\boldsymbol{\lambda}$ approximation (5) and neglecting second order terms yields the $\hat{h}_V$ description

$$\begin{aligned} \hat{h}_V = \mathbf{e}_z'\hat{\mathcal{R}}^{B}_{M}\mathbf{R}\mathbf{e}_z L_r &\approx \mathbf{e}_z'\left[\mathbf{I}_3 + (\delta\boldsymbol{\lambda})_\times\right]\mathcal{R}\,{}^{B}_{M}\mathbf{R}\mathbf{e}_z L_r \\ &\approx \mathbf{e}_z'\mathcal{R}\,{}^{B}_{M}\mathbf{R}\mathbf{e}_z(L+\delta L) - L_r\mathbf{e}_z'\left(\mathcal{R}\,{}^{B}_{M}\mathbf{R}\mathbf{e}_z\right)_\times\delta\boldsymbol{\lambda} \\ &= h_V + \mathbf{e}_z'\mathcal{R}\,{}^{B}_{M}\mathbf{R}\mathbf{e}_z\delta L - L_r\mathbf{e}_z'\left(\mathcal{R}\,{}^{B}_{M}\mathbf{R}\mathbf{e}_z\right)_\times\delta\boldsymbol{\lambda}, \end{aligned} \tag{22}$$

Combining (18-22), the measurement residual is described as a function of the EKF state variables as

$$\mathbf{z}_L = \mathbf{e}_z'\delta\mathbf{p} - L_r\mathbf{e}_z'\left(\mathcal{R}\,{}^{B}_{M}\mathbf{R}\mathbf{e}_z\right)_\times\delta\boldsymbol{\lambda} - h_S + \mathbf{e}_z'\mathcal{R}\,{}^{B}_{M}\mathbf{R}\mathbf{e}_z\mathbf{n}_L. \tag{23}$$

In practical applications, the landing and takeoff locations have different terrain height h_S. After the takeoff and during flight operations, the LASER sensor is switched off to prevent erroneous readings due to the terrain height fluctuations and to the interference of obstacles located between the vehicle and the ground. When the landing maneuver starts, the LASER is switched on to estimate the new h_S. A method to estimate h_S using the filter uncertainty is discussed in Section 5 and validated in Section 6.

5. Implementation

This section details the state space model of the EKF, that integrates the INS with the vehicle model and LASER aiding techniques. The state variables and measurement residuals of the aiding techniques described previously are formulated in the state model space. The differences between the external and internal vehicle model aiding techniques are evidenced, and the discretization of the continuous state space model is presented for the purpose of implementation.

The standard continuous-time state space model is described by

$$\dot{\mathbf{x}}_C = \mathbf{F}_C\left(\mathbf{x}_C\right)\mathbf{x}_C + \mathbf{G}_C\left(\mathbf{x}_C\right)\,\mathbf{n}_{x_C} + \mathbf{u}_C, \qquad \mathbf{z}_C = \mathbf{H}_C\left(\mathbf{x}_C\right)\,\mathbf{x}_C + \mathbf{n}_{z_C}, \tag{24}$$

where $\mathbf{x}_C$ is the state vector, $\mathbf{F}_C$ is the state dynamics matrix, $\mathbf{n}_{x_C}$ is the state noise transformed by matrix $\mathbf{G}_C$, $\mathbf{u}_C$ is the system input vector, and $\mathbf{z}$ is the state measurement, corrupted by the noise vector $\mathbf{n}_{z_C}$. The state and measurement noises are assumed zero-mean, Gaussian white noises with covariance matrices denoted by $\mathbf{Q}_C$ and $\mathbf{R}_C$, respectively.

The state dynamics and measurement residuals (24) of the EKF are determined by the choice of aiding techniques, and obtained by the concatenation of the state and measurement models of each aiding source. The systems derived in Section 2 and Section 3 are detailed next.

5.1. INS/EKF state model

The state model dynamics for the INS errors are obtained directly from (6). Let $\mathbf{x}_{\text{INS}} = (\mathbf{p}, \mathbf{v}, \mathcal{R}, \mathbf{a}_r, \boldsymbol{\omega}_r)$ denote the INS quantities, the state model dynamics of the EKF describing the INS errors are given by

$$\dot{\delta}\mathbf{x} = \mathbf{F}_I(\mathbf{x}_{\text{INS}})\delta\mathbf{x} + \mathbf{G}_I(\mathbf{x}_{\text{INS}})\mathbf{n}_{\text{INS}}, \tag{25}$$

where

$$\delta\mathbf{x} = \begin{bmatrix}\delta\mathbf{p}' & \delta\mathbf{v}' & \delta\boldsymbol{\lambda}' & \delta\mathbf{b}_a' & \delta\mathbf{b}_\omega'\end{bmatrix}', \quad \mathbf{n}_{\text{INS}} = \begin{bmatrix}\mathbf{n}_p' & \mathbf{n}_a' & \mathbf{n}_\omega' & \mathbf{n}_{b_a}' & \mathbf{n}_{b_\omega}'\end{bmatrix}',$$

$$\mathbf{F}_I(\mathbf{x}_{\text{INS}}) = \begin{bmatrix}\mathbf{0} & \mathbf{I}_3 & \mathbf{0} & \mathbf{0} & \mathbf{0}\\ \mathbf{0} & \mathbf{0} & -\left(\mathcal{R}\mathbf{a}_r\right)_\times & -\mathcal{R} & \mathbf{0}\\ \mathbf{0} & \mathbf{0} & \mathbf{0} & \mathbf{0} & -\mathcal{R}\\ \mathbf{0} & \mathbf{0} & \mathbf{0} & \mathbf{0} & \mathbf{0}\\ \mathbf{0} & \mathbf{0} & \mathbf{0} & \mathbf{0} & \mathbf{0}\end{bmatrix}, \quad \mathbf{G}_I(\mathbf{x}_{\text{INS}}) = \texttt{blkdiag}\left(\mathbf{I}_3, \mathcal{R}, \mathcal{R}, -\mathbf{I}_3, -\mathbf{I}_3\right),$$

where `blkdiag`(...) represents a block diagonal matrix, $\mathbf{n}_p \sim \mathcal{N}(\mathbf{0}, \mathbf{\Xi}_p)$ is a auxiliary Gaussian white noise associated to the position error estimate and the state noise covariance matrix is given by

$$\mathbf{Q}_{\text{INS}} = \texttt{blkdiag}(\mathbf{\Xi}_p, \mathbf{\Xi}_a, \mathbf{\Xi}_\omega, \mathbf{\Xi}_{b_a}, \mathbf{\Xi}_{b_\omega}).$$

The measurement model for the proposed VD and LASER aiding techniques are described in the ensuing, however additional information sources are considered. A GPS receiver and a magnetometer are integrated in the system using the measurement residuals

$$\mathbf{z}_{\text{GPS}} := \hat{\mathbf{p}} - \mathbf{p}_{\text{GPS}} \approx \delta\mathbf{p} - \mathbf{n}_{\text{GPS}}, \quad \mathbf{z}_m := {}^{E}\mathbf{m} - \hat{\mathcal{R}}\mathbf{m}_r \approx \left({}^{E}\mathbf{m}\right)_\times \delta\boldsymbol{\lambda} - \mathcal{R}\mathbf{n}_m, \tag{26}$$

where $\mathbf{p}_{\text{GPS}}$ is the position measured by the GPS unit, $\mathbf{m}_r$ is the magnetometer reading, ${}^{E}\mathbf{m}$ represents the Earth's magnetic field in Earth coordinates, and $\mathbf{n}_{\text{GPS}} \sim \mathcal{N}(\mathbf{0}, \mathbf{\Xi}_{\text{GPS}})$, $\mathbf{n}_m \sim \mathcal{N}(\mathbf{0}, \mathbf{\Xi}_m)$ are Gaussian white noises. For further details on the derivation of the measurement residuals (26), the reader is referred to (Britting, 1971; Markley, 2003).

5.2. Vehicle Model Aiding

The EKF state space model, formulated using (24), is obtained by concatenating the state space model (25) that describes the INS estimation errors, with the state model and measurements of the vehicle model aiding techniques described in Sections 3.2 and 3.3. With a slight abuse of notation, the EKF state model (24) is defined for the external and embedded vehicle model dynamics using the same state $\mathbf{x}_C$ and measurement $\mathbf{z}_C$.

5.2.1. External Vehicle Model Aiding

In the external vehicle model aiding technique, the vehicle dynamics are computed by a self-contained VD simulator, and the INS and the VD states are distinct. As a mean to estimate and compensate for the INS errors, the EKF state model is augmented with the VD error dynamics (10), and the measurement residuals (12) are a linear combination of the INS and the VD errors. The classical VD aiding methodology requires specific computational routines to estimate and compensate for the estimation errors of the VD simulator.

The continuous-time error state space model for the navigation system with external VD aiding is obtained directly from the EKF/INS state model (25) augmented by the VD error dynamics (10), yielding

$$\mathbf{x}_C := \begin{bmatrix} \delta\mathbf{x}' & \delta\mathbf{x}_V' \end{bmatrix}', \qquad \mathbf{n}_{x_C} := \begin{bmatrix} \mathbf{n}_{\text{INS}}' & \mathbf{n}_{x_V}' \end{bmatrix}', \qquad \mathbf{u}_C = \mathbf{0},$$

$$\mathbf{F}_C(\mathbf{x}_{\text{INS}}, \mathbf{x}_V) = \begin{bmatrix} \mathbf{F}_I(\mathbf{x}_{\text{INS}}) & \mathbf{0}_{15\times 9} \\ \mathbf{0}_{9\times 15} & \mathbf{F}_V(\mathbf{x}_V) \end{bmatrix}, \qquad \mathbf{G}_C(\mathbf{x}_{\text{INS}}) = \begin{bmatrix} \mathbf{G}_I(\mathbf{x}_{\text{INS}}) & \mathbf{0}_{15\times 9} \\ \mathbf{0}_{9\times 15} & \mathbf{G}_V \end{bmatrix},$$

with the vehicle states, noises and model submatrices given by

$$\delta\mathbf{x}_V := \begin{bmatrix} \delta\boldsymbol{\omega}'_V & \delta^B\mathbf{v}'_V & \delta\boldsymbol{\lambda}'_V \end{bmatrix}', \qquad \mathbf{n}_{x_V} := \begin{bmatrix} \mathbf{n}'_{\boldsymbol{\omega}_V} & \mathbf{n}'_{\mathbf{v}_V} & \mathbf{n}'_{\boldsymbol{\lambda}_V} \end{bmatrix}',$$

$$\mathbf{F}_V(\mathbf{x}_V) = \begin{bmatrix} \frac{\partial f_\omega}{\partial \boldsymbol{\omega}} & \mathbf{0} & \mathbf{0} \\ \frac{\partial f_v}{\partial \boldsymbol{\omega}} & \frac{\partial f_v}{\partial^B \mathbf{v}} & \frac{\partial f_v}{\partial \boldsymbol{\lambda}} \\ \mathcal{R}_V & \mathbf{0} & \mathbf{0} \end{bmatrix}\Bigg|_{\mathbf{x}_V}, \qquad \mathbf{G}_V = \begin{bmatrix} \mathbf{I} & \mathbf{0} & \mathbf{0} \\ \mathbf{0} & \mathbf{I} & \mathbf{0} \\ \mathbf{0} & \mathbf{0} & \mathbf{I} \end{bmatrix},$$

where $\mathbf{n}_{\boldsymbol{\omega}_V}$, $\mathbf{n}_{\mathbf{v}_V}$, and $\mathbf{n}_{\boldsymbol{\lambda}_V}$ are auxiliary zero-mean, Gaussian white noises with covariances $\boldsymbol{\Xi}_{\boldsymbol{\omega}_V}$, $\boldsymbol{\Xi}_{\mathbf{v}_V}$, and $\boldsymbol{\Xi}_{\boldsymbol{\lambda}_V}$ respectively, that characterize the vehicle modeling errors.

The measurement residuals (12) are a function of the INS and VD errors, given in the state space form by

$$\mathbf{z}_C := \begin{bmatrix} \mathbf{z}'_\omega & \mathbf{z}'_u & \mathbf{z}'_{\mathcal{R}} \end{bmatrix}', \quad \mathbf{n}_{z_V} := \begin{bmatrix} \mathbf{n}'_\omega + \mathbf{n}'_{\mathbf{z}_\omega} & \mathbf{n}'_{\mathbf{z}_u} & \mathbf{n}'_{\mathbf{z}_\mathcal{R}} \end{bmatrix}',$$

$$\mathbf{H}_C(\mathbf{x}_{\text{INS}}) = \begin{bmatrix} \mathbf{0} & \mathbf{0} & \mathbf{0} & \mathbf{0} & -\mathbf{I} & -\mathbf{I} & \mathbf{0} & \mathbf{0} \\ \mathbf{0} & \mathcal{R}' & \mathcal{R}'(\mathbf{v})_\times & \mathbf{0} & \mathbf{0} & \mathbf{0} & -\mathbf{I} & \mathbf{0} \\ \mathbf{0} & \mathbf{0} & \mathbf{I} & \mathbf{0} & \mathbf{0} & \mathbf{0} & \mathbf{0} & -\mathbf{I} \end{bmatrix},$$

where $\mathbf{n}_{z_\omega}$, $\mathbf{n}_{z_U}$, and $\mathbf{n}_{z_\mathcal{R}}$ are a auxiliary zero-mean Gaussian white noises associated to the $\delta\mathbf{z}_V$ observation, with covariances $\boldsymbol{\Xi}_{z_\omega}$, $\boldsymbol{\Xi}_{z_U}$, and $\boldsymbol{\Xi}_{z_\mathcal{R}}$ respectively. The vehicle states and measurements noise covariance matrices are

$$\mathbf{Q}_C = \text{blkdiag}(\mathbf{Q}_{\text{INS}}, \boldsymbol{\Xi}_{\omega_V}, \boldsymbol{\Xi}_{u_V}, \boldsymbol{\Xi}_{\mathcal{R}_V}), \qquad \mathbf{R}_C = \text{blkdiag}(\boldsymbol{\Xi}_{z_\omega} + \boldsymbol{\Xi}_\omega, \boldsymbol{\Xi}_{z_u}, \boldsymbol{\Xi}_{z_\mathcal{R}}),$$

where the auxiliary white noise variances account for the effects of neglecting second order terms and unmodeled uncertainties in the measurement residual derivation.

The observation $\mathbf{z}_\omega$ is disturbed by rate gyro noise, so a state and measurement noise correlation matrix is introduced in the Kalman filter equations

$$\mathbf{C}_C = \begin{bmatrix} \mathbf{0} & \mathbf{0} & \boldsymbol{\Xi}_\omega & \mathbf{0} & \mathbf{0} & \mathbf{0}_{3\times 9} \\ & & \mathbf{0}_{6\times 15} & & & \mathbf{0}_{6\times 9} \end{bmatrix}',$$

for details on the definition and derivation see (Brown and Hwang, 1997) and references therein.

5.2.2. Embedded Vehicle Model Aiding

In the embedded vehicle model aiding technique, the EKF state model is augmented with the VD error dynamics (13), which are propagated using the INS estimates, and updated by the Kalman filter algorithm. The measurements are obtained from the INS inertial estimates, given the residuals (12). The continuous-

time state space model is given by

$$\mathbf{x}_C := \begin{bmatrix} \delta\mathbf{x}' & \mathbf{x}_V' \end{bmatrix}', \quad \mathbf{n}_{x_C} := \begin{bmatrix} \mathbf{n}_{\text{INS}}' & \mathbf{n}_{x_V}' \end{bmatrix}', \quad \mathbf{u}_C = \begin{bmatrix} f_\omega(\boldsymbol{\omega}, \mathbf{N}_{th})' & f_v(\boldsymbol{\omega}, {}^B\mathbf{v}, \mathcal{R}, \mathbf{F}_{th})' \end{bmatrix}',$$

$$\mathbf{F}_C(\mathbf{x}_{\text{INS}}) = \begin{bmatrix} \mathbf{F}_I(\mathbf{x}_{\text{INS}}) & \mathbf{0}_{15\times 6} \\ \mathbf{F}_V(\mathbf{x}_{\text{INS}}) & \mathbf{0}_{6\times 6} \end{bmatrix}, \quad \mathbf{G}_C(\mathbf{x}_{INS}) = \begin{bmatrix} \mathbf{G}_I(\mathbf{x}_{\text{INS}}) & \mathbf{0}_{9\times 6} \\ \mathbf{G}_V(\mathbf{x}_{\text{INS}}) & \mathbf{I}_6 \end{bmatrix},$$

where

$$\mathbf{x}_V = \begin{bmatrix} \boldsymbol{\omega}' & {}^B\mathbf{v}' \end{bmatrix}', \quad \mathbf{n}_{x_V} = \begin{bmatrix} \mathbf{n}_{\boldsymbol{\omega}_V}' & \mathbf{n}_{{}^B\mathbf{v}_V}' \end{bmatrix}',$$

$$\mathbf{F}_V(\mathbf{x}_{\text{INS}}) = \begin{bmatrix} \mathbf{0} & \mathbf{0} & \mathbf{0} & \mathbf{0} & \frac{\partial f_\omega}{\partial \boldsymbol{\omega}} \\ \mathbf{0} & -\frac{\partial f_v}{\partial {}^B\mathbf{v}}\mathcal{R}' & -\left(\frac{\partial f_v}{\partial \delta\boldsymbol{\lambda}} + \frac{\partial f_v}{\partial {}^B\mathbf{v}}\mathcal{R}'\left(\mathbf{v}\right)_\times\right) & \mathbf{0} & \frac{\partial f_v}{\partial \boldsymbol{\omega}} \end{bmatrix}\Bigg|_{\hat{\mathbf{x}}},$$

$$\mathbf{G}_V(\mathbf{x}_{\text{INS}}) = \begin{bmatrix} \mathbf{0} & \mathbf{0} & -\frac{\partial f_\omega}{\partial \boldsymbol{\omega}} & \mathbf{0} & \mathbf{0} \\ \mathbf{0} & \mathbf{0} & -\frac{\partial f_v}{\partial \boldsymbol{\omega}} & \mathbf{0} & \mathbf{0} \end{bmatrix}\Bigg|_{\hat{\mathbf{x}}},$$

where $\mathbf{n}_{\boldsymbol{\omega}_V}$ and $\mathbf{n}_{{}^B\mathbf{v}_V}$ are auxiliary zero-mean, Gaussian white noises with covariances $\boldsymbol{\Xi}_{\boldsymbol{\omega}_V}$ and $\boldsymbol{\Xi}_{{}^B\mathbf{v}_V}$ that characterize the vehicle modeling errors. The $\mathbf{x}_V$ state variable is propagated using the INS estimates as expressed in (13), and the EKF state matrices depend only on the INS quantities $\mathbf{x}_{\text{INS}}$, as expected from the derivation of the technique presented in Section 3.3.

The measurement state model (14) is described in the state space form by

$$\mathbf{z} := \begin{bmatrix} \mathbf{z}_\omega' & \mathbf{z}_u' \end{bmatrix}', \quad \mathbf{n}_{z_V} := \begin{bmatrix} \mathbf{n}_\omega' + \mathbf{n}_{\mathbf{z}_\omega}' & \mathbf{n}_{\mathbf{z}_u}' \end{bmatrix}',$$

$$\mathbf{H}_C(\mathbf{x}_{INS}) = \begin{bmatrix} \mathbf{0} & \mathbf{0} & \mathbf{0} & \mathbf{0} & -\mathbf{I} & \mathbf{I} & \mathbf{0} \\ \mathbf{0} & \mathcal{R}' & \mathcal{R}'\left(\mathbf{v}\right)_\times & \mathbf{0} & \mathbf{0} & \mathbf{0} & \mathbf{I} \end{bmatrix},$$

and $\mathbf{n}_{\mathbf{z}_\omega} \sim \mathcal{N}(\mathbf{0}, \boldsymbol{\Xi}_{z_\omega})$ and $\mathbf{n}_{\mathbf{z}_u} \sim \mathcal{N}(\mathbf{0}, \boldsymbol{\Xi}_{z_u})$ are auxiliary zero-mean Gaussian white noises associated with the measurement. The vehicle states and measurements noise covariance and covariance correlation matrices are

$$\mathbf{Q}_C = \text{blkdiag}(\mathbf{Q}_{\text{INS}}, \boldsymbol{\Xi}_{\omega_V}, \boldsymbol{\Xi}_{u_V}), \mathbf{R}_C = \text{blkdiag}(\boldsymbol{\Xi}_{z_\omega} + \boldsymbol{\Xi}_\omega, \boldsymbol{\Xi}_{z_u}),$$

$$\mathbf{C}_C = \begin{bmatrix} \mathbf{0} & \mathbf{0} & \boldsymbol{\Xi}_\omega & \mathbf{0} & \mathbf{0} & \mathbf{0}_{3\times 6} \\ & & \mathbf{0}_{3\times 15} & & & \mathbf{0}_{3\times 6} \end{bmatrix}'.$$

5.3. LASER Aiding

The LASER sensor is integrated with the INS by defining the variables and matrices of the EKF state model (24) as

$$\mathbf{x}_C := \begin{bmatrix} \delta\mathbf{x}' & h_S \end{bmatrix}', \quad \mathbf{n}_{x_C} := \begin{bmatrix} \mathbf{n}_{\text{INS}}' & n_{h_S} \end{bmatrix}', \quad \mathbf{u}_C = \mathbf{0},$$

$$\mathbf{F}_C(\mathbf{x}_{\text{INS}}) = \begin{bmatrix} \mathbf{F}_I(\mathbf{x}_{\text{INS}}) & \mathbf{0}_{15\times 1} \\ \mathbf{0}_{1\times 15} & 0 \end{bmatrix}, \quad \mathbf{G}_C(\mathbf{x}_{\text{INS}}) = \begin{bmatrix} \mathbf{G}_I(\mathbf{x}_{\text{INS}}) & \mathbf{0}_{9\times 1} \\ \mathbf{0}_{1\times 9} & 1 \end{bmatrix}.$$

The measurement model is obtained from (23) and given by

$$\mathbf{z}_C := \mathbf{z}_L, \quad \mathbf{n}_{z_C} := \mathbf{n}_{z_L},$$
$$\mathbf{H}_C(\mathbf{x}_{\text{INS}}) = \begin{bmatrix} \mathbf{e}_z' & \mathbf{0}_{1\times 3} & -\mathbf{e}_z' \left(\mathcal{R}\,{}_M^B \mathbf{R}\mathbf{e}_z\right)_\times & \mathbf{0}_{1\times 3} & \mathbf{0}_{1\times 3} & -1 \end{bmatrix},$$

where

$$\mathbf{Q}_C = \text{blkdiag}(\mathbf{Q}_{\text{INS}}, \Xi_{h_S}), \qquad \mathbf{R}_C = (\mathbf{e}_z' \mathcal{R}\,{}_M^B \mathbf{R}\mathbf{e}_z)^2 \Xi_L, \qquad \mathbf{C}_C = \mathbf{0}.$$

The LASER sensor is adopted for takeoff and landing maneuvers and to determine the relative position to structures. Previous to the LASER's activation, the estimation covariance of h_S is defined large enough to account for the uncertainty in the terrain height. When the LASER sensor is activated, the EKF recursively estimates the terrain height h_S based on the sensor measurements, and the uncertainty on the terrain's height converges asymptotically to a steady state value, that depends on the sensor's accuracy.

When the LASER is switched off, the uncertainty on the terrain height h_S will grow at a rate defined by the noise covariance Ξ_{h_S}. Techniques to avoid numerical problems in the EKF covariance matrices should be adopted, namely square root filtering (Brown and Hwang, 1997) or by setting $\Xi_{h_S} = 0$ if the uncertainty reaches a prespecified upper bound.

5.4. State Model Discretization

The discrete-time state space model

$$\mathbf{x}_{k+1} = \Phi_k \mathbf{x}_k + \mathbf{w}_k, \quad \mathbf{z}_k = \mathbf{H}_k \mathbf{x}_k + \mathbf{v}_k,$$

is obtained using the zero order hold discretization technique (Brown and Hwang, 1997), and is given by

$$\mathbf{\Phi}_k = e^{\mathbf{F}_k T}, \quad \mathbf{H}_k = \mathbf{H}_C|_{t=t_k},$$

and the discrete-time noise covariance matrices are described by

$$\mathbf{Q}_k \simeq [\mathbf{G}_k \mathbf{Q}_C \mathbf{G}_k']T, \quad \mathbf{R}_k \simeq \frac{\mathbf{R}_{Ck}}{T},$$
$$\mathbf{C}_k = \frac{1}{T}\int_{t_{k-1}}^{t_k} \mathbf{\Phi}(t_{k+1}, \theta)\mathbf{G}_C(\tau)\mathbf{C}_C(\tau)d\tau \approx (\mathbf{I} + \frac{\mathbf{F}_k T}{2} + \frac{\mathbf{F}_k^2 T^2}{6})\mathbf{G}_k \mathbf{C}_{Ck},$$

where T is the sampling period, $\mathbf{F}_k = \mathbf{F}_C|_{t=t_k}$, $\mathbf{G}_k = \mathbf{G}_C|_{t=t_k}$, $\mathbf{R}_{Ck} = \mathbf{R}_C|_{t=t_k}$, $\mathbf{C}_{Ck} = \mathbf{C}_C|_{t=t_k}$and $\mathbf{\Phi}_k = \mathbf{\Phi}(t_{k+1}, t_k)$ denotes the state transition matrix.

5.5. Error Compensation Routines

In the current direct feedback configuration, the EKF error estimates are compensated in the INS moderate-speed algorithm, using

$$\mathbf{p}_k^+ = \mathbf{p}_k^- - \delta\hat{\mathbf{p}}_k, \qquad \mathbf{v}_k^+ = \mathbf{v}_k^- - \delta\hat{\mathbf{v}}_k, \qquad \mathcal{R}_k^+ = \mathcal{R}'(\delta\hat{\boldsymbol{\lambda}}_k)\mathcal{R}_k^-,$$
$$\mathbf{b}_{a\,k}^+ = \mathbf{b}_{a\,k} - \delta\hat{\mathbf{b}}_{a\,k}, \qquad \mathbf{b}_{\omega\,k}^+ = \mathbf{b}_{\omega\,k}^- - \delta\hat{\mathbf{b}}_{\omega\,k}, \tag{27}$$

where matrix $\mathcal{R}'(\delta\hat{\boldsymbol{\lambda}}_k)$ is implemented using power series expansion of trigonometric terms up to an arbitrary accuracy (Savage, 1998a). The EKF error estimates are reset after being applied to compensate the INS states, that updates the linearization point and keeps filter perturbational dynamics valid under the first order assumptions.

Similar to the INS error compensation routines (27), the estimated VD errors are fed back to the external vehicle simulator, as shown in Fig. 1(a), using the following error compensation routines

$$\boldsymbol{\omega}^+_{V\,k} = \boldsymbol{\omega}^-_{V\,k} - \delta\hat{\boldsymbol{\omega}}_{V\,k}, \quad {}^B\mathbf{v}^+_{V\,k} = {}^B\mathbf{v}^-_{V\,k} - \delta^B\hat{\mathbf{v}}_{V\,k}, \quad \mathcal{R}^+_{V\,k} = \mathcal{R}'_{V\,k}(\delta\hat{\boldsymbol{\lambda}}_V)\mathcal{R}^-_{V\,k}. \tag{28}$$

By construction, the internal VD technique propagates the vehicle dynamics using the EKF state space. The estimation error compensation is automatically performed by the EKF in the state update step, and vehicle model error compensation routines are not necessary in this technique.

6. Simulation Results

This section presents the simulations results that validate and illustrate the properties of the proposed aiding techniques. The integration of the VD and LASER range finder information in the navigation system is studied using three simulation setups. The first simulation compares the estimation results of the VD aided navigation system with those of a classical GPS/INS architecture, for a 6-DOF rigid body describing a trimming trajectory. Bias and velocity estimation enhancements are discussed, and the internal VD aiding technique is validated with respect to the classical VD aided navigation system.

In the second simulation, the application of the VD aiding for highly nonlinear, realistic vehicle models is demonstrated for a model-scale Vario X-Treme helicopter. The proposed embedded VD aiding technique is adopted, and simulation results are presented for a takeoff and turning trajectory. The estimation results are depicted for GPS based and VD aided navigation architectures, and the estimated error covariance is shown to evidence the accuracy improvements.

The third simulation emphasizes the role of the LASER range finder sensor for critical maneuvers. The vehicle describes a hovering maneuver, and has to acquire the distance to ground for precise landing. Accuracy improvements obtained with the LASER range finder sensor integrated on a GPS/INS configuration are evidenced. Dynamic estimation of distance to ground is performed, and position and velocity vertical channel accuracy enhancements are shown.

The INS high speed algorithm is set to run at 100 Hz and the normal speed algorithm is synchronized with the EKF, both executed at 50Hz. The LASER sensor operates at 10Hz and the GPS provides position measurements at the nominal frequency of 1Hz. The characteristics of the sensors non-idealities are presented in Table 1.

Table 1: Sensor Non-idealities

Sensor	**Bias**	**Noise Variance**
Rate Gyro	0.05 °/s	$(0.02\ ^\circ/\text{s})^2$
Accelerometer	10 mg	$(0.6\ \text{mg})^2$
LASER	-	$(10^{-2}\ \text{m})^2$
Magnetometer	-	$(1\ \text{mG})^2$
GPS	-	$10\ \text{m}^2$

Table 2: Rigid Body Characteristics

Property	**Nominal Value**
Mass	$m = 10$ Kg
Length, Width, Height	$(l, w, h) = (1.00, 0.75, 0.25)$ m
Rear Thrusters	${}^B\mathbf{p}_{\text{th}\,1,2} = (-0.50, \pm 0.30, 0)$ m
Side Thrusters	${}^B\mathbf{p}_{\text{th}\,3,4} = (0, -0.375, \pm 0.10)$ m
Bottom Thrusters	${}^B\mathbf{p}_{\text{th}\,5,6} = (\pm 0.40, 0, -0.125)$ m
Damping Coefficients	$K_{\text{ang}} = 4$, $K_{\text{lin}} = 2$

6.1. Vehicle Model Aiding

The VD aiding technique is validated using the 6-DOF rigid body model described in Section 3.1, with the parameters detailed in Table 2. The external VD, embedded VD and a classical GPS/INS architecture results are obtained for the rigid body model subject to constant linear and centripetal acceleration, describing the upwards trimming trajectory shown in Fig. 3. The bias estimation and compensation is analyzed by considering a 30% bias calibration error in each channel of the accelerometer and rate gyro sensors.

The linear and angular velocity information provided by the vehicle model clearly endows the filter to compensate for the inertial sensor biases, as shown in Figure 4. Velocity estimation results are enhanced, and bias calibration errors are promptly tackled by the VD aided navigation system, yielding smaller bias estimation error. Although position and attitude information is not directly provided for by the vehicle model, attitude estimates are more accurate with VD aiding, as shown in Table 3, due to the smaller velocity and bias estimation errors.

The integration of the VD model with other aiding sensors is demonstrated by including a magnetometer in the navigation system, using the measurement residual (26). The use of a magnetometer is motivated by the poor yaw estimation evidenced in Table 3, which is justified by analyzing the correlation of the attitude and velocity errors in (6). The term in (6) that correlates velocity and attitude errors satisfies

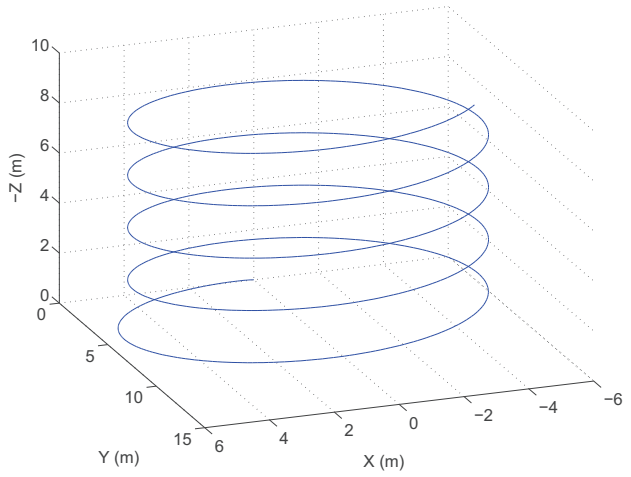

Figure 3: Rigid body trimming trajectory

Table 3: Attitude estimation error (Rigid body, Magnetometer off)

	RMS Error		
Aiding information	Yaw (°)	Pitch (°)	Roll (°)
GPS	1.73	0.14	0.13
Ext. VD	0.11	2.47×10^{-2}	3.73×10^{-2}
Int. VD	0.15	2.33×10^{-2}	3.83×10^{-2}

$(\mathcal{R}\mathbf{a}_r)_\times \mathbf{e}_z \approx \mathbf{0}$ for the trimming trajectory of Figure 3, where the vehicle rotates only about the z axis. Position observations that aid velocity estimation do not yield any update on $\delta\lambda_z$, which shows that the yaw angle is hard to determine using only GPS measurements for the described trajectory.

Using the magnetometer improves estimation results of the GPS based and VD aided navigation systems, as seen by comparing Fig. 4 with Fig. 5, and Table 3 with Table 4. Position and velocity estimation errors are presented in Tables 5, and 6 respectively. The estimation errors obtained with the VD aiding are smaller that those obtained with the GPS aiding, independently of using the magnetometer. Improving the velocity and bias estimation errors using the vehicle model information also reduces the attitude and position estimation errors.

The performance of the embedded and the external VD architectures are similar, which validates the proposed aiding technique. Both architectures use the same vehicle model, and hence the aiding information introduced in the filter is the same, and the estimation results are thus similar. However, the computational savings and flexibility associated with the proposed VD aiding technique are obtained without affecting the navigation system accuracy, which supports the embedded VD approach.

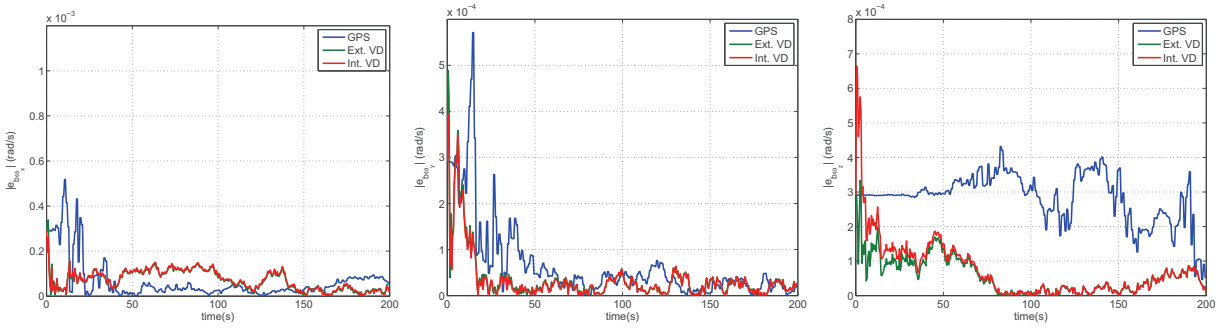

(a) Rate Gyro Bias ($\mathbf{b}_{\omega x}$) (b) Rate Gyro Bias ($\mathbf{b}_{\omega y}$) (c) Rate Gyro Bias ($\mathbf{b}_{\omega z}$)

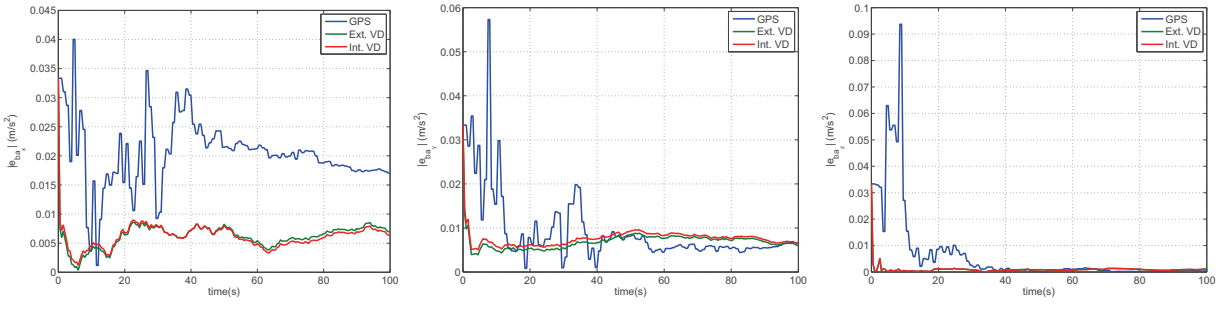

(d) Accelerometer Bias ($\mathbf{b}_{a\,x}$) (e) Accelerometer Bias ($\mathbf{b}_{a\,y}$) (f) Accelerometer Bias ($\mathbf{b}_{a\,z}$)

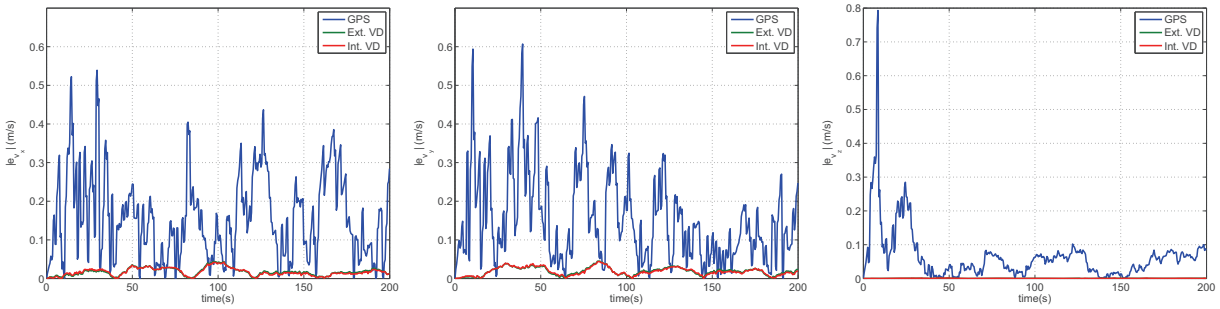

(g) Velocity ($\mathbf{v}_x$) (h) Velocity ($\mathbf{v}_y$) (i) Velocity ($\mathbf{v}_z$)

Figure 4: Estimation errors of the GPS and the VD aided navigation systems (Rigid body, Magnetometer off)

Table 4: Attitude estimation error (Rigid Body, Magnetometer on)

	RMS Error		
Aiding information	Yaw (°)	Pitch (°)	Roll (°)
GPS	1.35×10^{-2}	8.96×10^{-2}	8.02×10^{-2}
Ext. VD	1.22×10^{-2}	1.69×10^{-2}	1.75×10^{-2}
Int. VD	1.22×10^{-2}	1.81×10^{-2}	1.80×10^{-2}

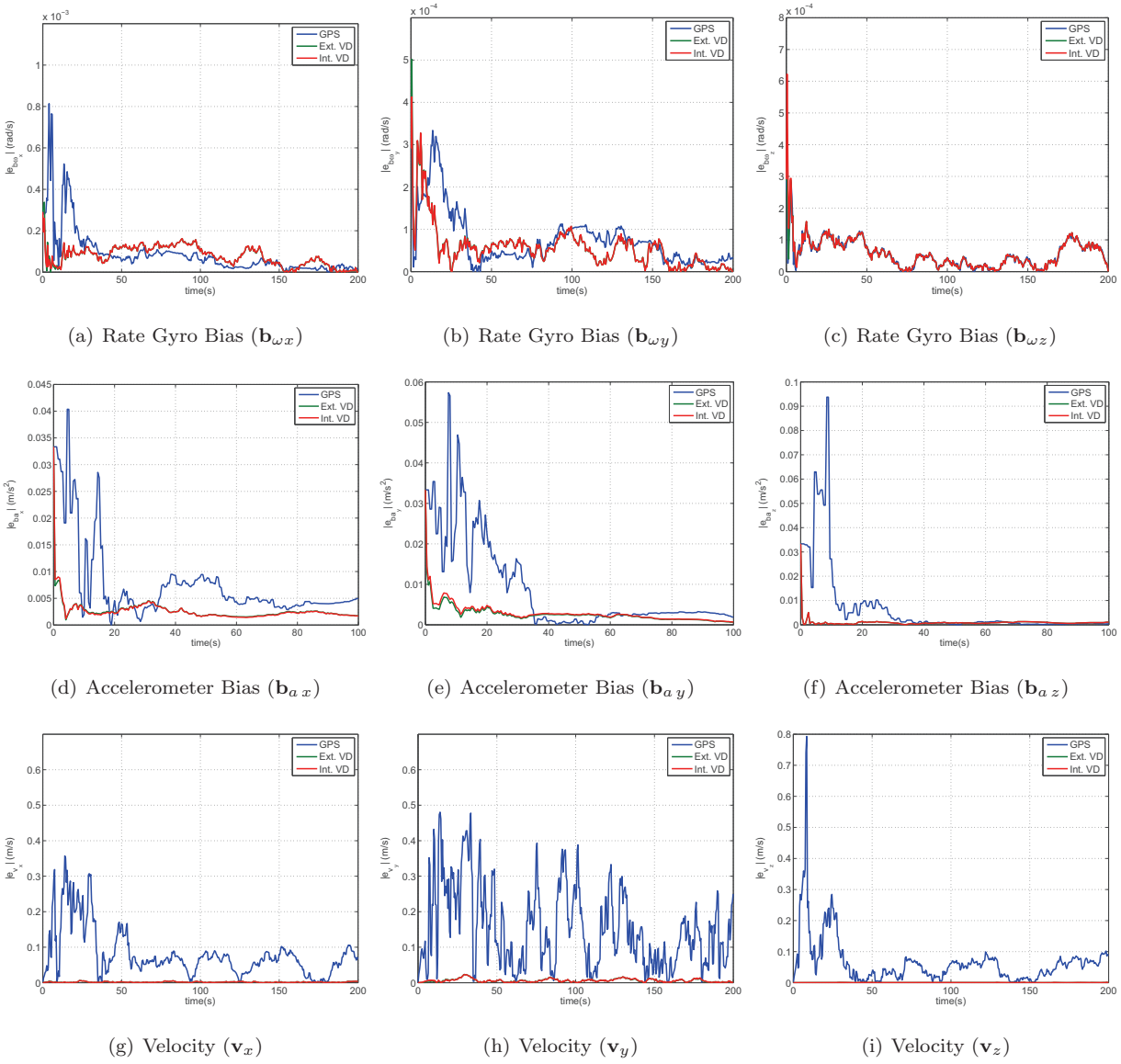

(a) Rate Gyro Bias ($\mathbf{b}_{\omega x}$) (b) Rate Gyro Bias ($\mathbf{b}_{\omega y}$) (c) Rate Gyro Bias ($\mathbf{b}_{\omega z}$)

(d) Accelerometer Bias ($\mathbf{b}_{a\,x}$) (e) Accelerometer Bias ($\mathbf{b}_{a\,y}$) (f) Accelerometer Bias ($\mathbf{b}_{a\,z}$)

(g) Velocity ($\mathbf{v}_x$) (h) Velocity ($\mathbf{v}_y$) (i) Velocity ($\mathbf{v}_z$)

Figure 5: Estimation errors of the GPS and the VD aided navigation systems (Rigid body, Magnetometer on)

Table 5: Position estimation error (Rigid body, Magnetometer on)

	RMS Error		
Aiding information	p_x (m)	p_y (m)	p_z (m)
GPS	0.95	1.17	1.07
Ext. VD	4.00×10^{-2}	0.10	1.88×10^{-2}
Int. VD	5.06×10^{-2}	9.87×10^{-2}	1.84×10^{-2}

Table 6: Velocity estimation error (Rigid body, Magnetometer on)

	RMS Error		
Aiding information	v_x (m/s)	v_y (m/s)	v_z (m/s)
GPS	0.10	0.19	0.10
Ext. VD	2.08×10^{-3}	7.57×10^{-3}	4.32×10^{-4}
Int. VD	2.06×10^{-3}	7.61×10^{-3}	4.49×10^{-4}

Figure 6: Vario X-treme model-scale helicopter

6.2. Vario X-Treme Helicopter

The 6-DOF rigid body was adopted to illustrate and validate the proposed aiding technique due to its simplicity, but it does not qualify as a realistic air vehicle. In this section, simulation results are presented for the Vario X-Treme helicopter, depicted in Fig. 6. This autonomous vehicle features a six degrees of freedom rigid body dynamic model driven by external forces and moments that encompass the main rotor and tail rotor effects, including the first order blade pitching dynamics with Bell-Hiller mechanism and the steady-state blade flapping dynamics. The model dynamics, derived from first-principles in (Cunha and Silvestre, 2003; Guerreiro, 2005), are summarized in Appendix A. The considered model, although simplified, is highly nonlinear and coupled, and is adopted to take a step towards the implementation of the internal VD aiding technique in field applications.

The simulated takeoff trajectory, depicted in Fig. 7, consists of an ascending turn, followed by a straight upwards path. A 30% bias calibration error is assumed and the magnetometer is used to compensate for the yaw observability.

Although the Vario X-treme model is highly nonlinear, the combination of the internal VD aiding with the linear extended Kalman filtering yields accurate attitude, velocity, and position estimates, as presented in Tables 7, 8, and 9 respectively. The helicopter model aiding enhances the INS estimates, as shown in the position results of Fig. 8 and in the bias and velocity errors illustrated in Fig. 9. The filter estimated error covariance is, in general, consistent with the estimation errors.

The position results in Fig. 9 and Table 9 show that the VD aiding technique effectively enhances the tra-

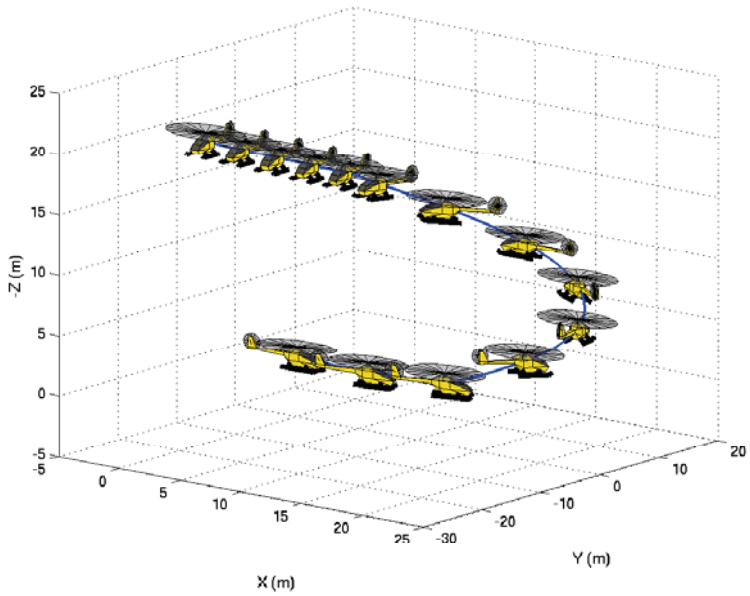

Figure 7: Vario X-treme simulated trajectory

Table 7: Attitude estimation error (Vario X-treme helicopter)

	RMS error		
Aiding information	Yaw (°)	Pitch (°)	Roll (°)
GPS	1.26×10^{-2}	9.15×10^{-2}	7.95×10^{-2}
Vario X-Treme Model	1.27×10^{-2}	2.10×10^{-2}	1.31×10^{-2}

Table 8: Velocity estimation error (Vario X-treme helicopter)

	RMS error		
Aiding information	v_x (m/s)	v_y (m/s)	v_z (m/s)
GPS	0.13	0.26	0.20
Vario X-Treme Model	2.65×10^{-2}	9.62×10^{-3}	3.75×10^{-3}

Table 9: Position estimation error (Vario X-treme helicopter)

	RMS error		
Aiding information	p_x (m)	p_y (m)	p_z (m)
GPS	1.15	1.46	1.55
Vario X-Treme Model	0.23	5.71×10^{-2}	0.20

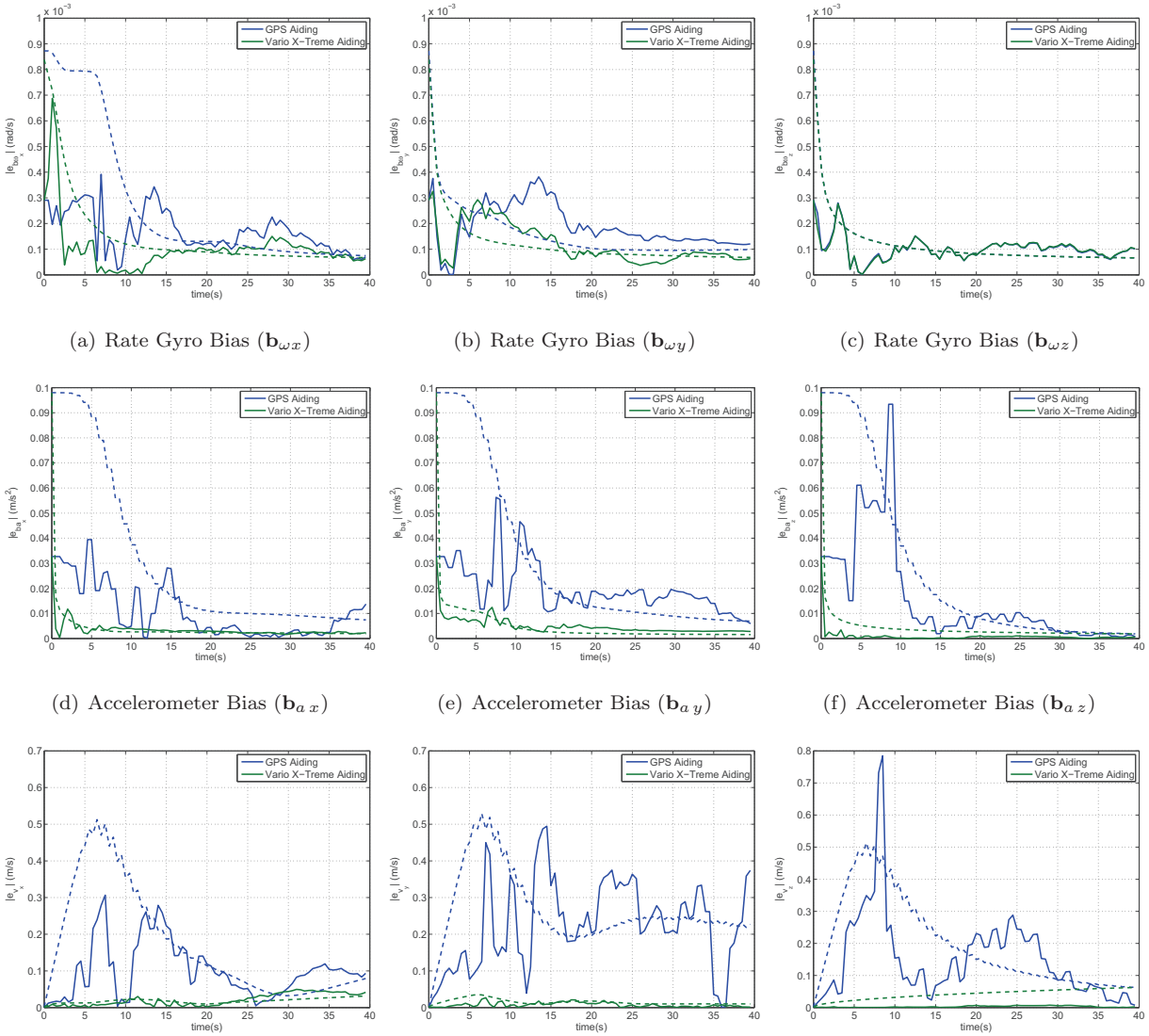

(a) Rate Gyro Bias ($\mathbf{b}_{\omega x}$) (b) Rate Gyro Bias ($\mathbf{b}_{\omega y}$) (c) Rate Gyro Bias ($\mathbf{b}_{\omega z}$)

(d) Accelerometer Bias ($\mathbf{b}_{a\,x}$) (e) Accelerometer Bias ($\mathbf{b}_{a\,y}$) (f) Accelerometer Bias ($\mathbf{b}_{a\,z}$)

(g) Velocity ($\mathbf{v}_x$) (h) Velocity ($\mathbf{v}_y$) (i) Velocity ($\mathbf{v}_z$)

Figure 8: Vario X-treme VD vs GPS aiding estimation errors (solid line) and estimated error standard deviation (dashed line)

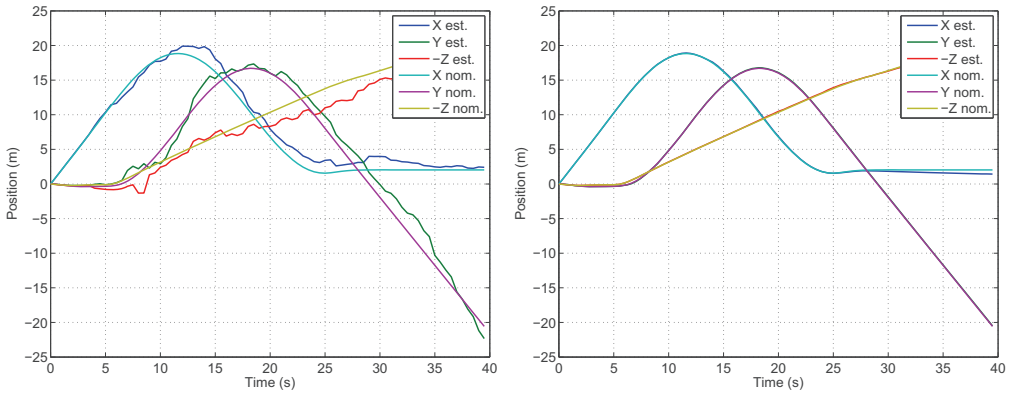

(a) GPS aiding

(b) Vario X-treme model aiding

Figure 9: Trajectory estimation for the Vario X-treme

jectory estimation to a submetric accuracy. As discussed in (Julier and Durrant-Whyte, 2003; Koifman and Bar-Itzhack, 1999), the VD aiding results must be addressed with care. Vehicle modeling errors, model simplification assumptions or unmodeled time-varying parameters, perturbations and dynamics, such as vehicle load and wind gusts, may severely affect the navigation system performance if not correctly accounted for in the filter.

The tuning of the noise covariance matrices, the estimation of additional states and parameters and the use of more accurate vehicle model dynamics, among other techniques (Julier and Durrant-Whyte, 2003), are adopted to allow for the use of VD in real navigation systems. Nonetheless, side effects such as the poor observability of the augmented states, the over-parametrization of the vehicle model or even the inability to obtain a vehicle model which yields information on the real vehicle dynamics may occur. The use of the full VD model in filtering is a time-consuming process, requiring navigation systems engineering expertise for complex vehicles.

Encouraging experimental results with the HUGIN 4500 underwater vehicle have been recently reported in (Hegrenaes et al., 2008). Also, exploiting simple vehicle motion constraints yields noticeable accuracy improvements in the experimental results presented in (Dissanayake and Sukkarieh, 2001) for a land vehicle. These practical results evidence that either full, or simplified, vehicle models can effectively enhance the estimation results of GPS/INS architectures. The integration of the vehicle dynamics in the navigation system is a valuable aiding technique, especially suited for the cases of GPS outage or jamming and when other external sensors are not available or provide poor observability of the vehicle states.

6.3. LASER Aiding

The LASER range sensor implementation is analyzed for a landing operation of an air vehicle equipped with a standard GPS/INS unit. The vehicle hovers the landing zone, as illustrated in Fig. 2, and activates the LASER at $t = 20$ s to acquire an accurate distance-to-ground estimate. The terrain height is $h_S = 4$ m, the

LASER is oriented along the z axis of the body frame, that is ${}^{B}_{M}\mathbf{R} = \mathbf{I}$, and the sensor noise is characterized in Table 1.

The estimation results depicted in Fig. 10 show that the LASER sensor brings about accurate position and velocity estimates in the z axis, whereas using solely the GPS sensor yields high uncertainty on the position estimate, which may render landing unfeasible. The velocity and distance to ground estimation errors, illustrated in Figs.10(b) and 10(d) respectively, are reduced almost instantly when the LASER is activated. The same decrease is verified in the position estimation error, shown in 10(a), however the terrain height h_S is known with an uncertainty of 0.1 m, as depicted in Fig. 10(c). If the uncertainty about the terrain height is larger, then the position estimate error will converge slower to smaller values, as illustrated in Fig. 11 for an initial h_S uncertainty of 1 m.

This behavior is justified by noting that h_S is reconstructed using (15), (16), and accurate LASER range measurements that bring about precise h_V estimates. If little is known about h_S, then (16) implies that the uncertainty of h_S and of p_z are identical, and the filter can reduce the uncertainty only by using the model (15), that is a low frequency process, and hence $\hat{h}_S$ and $\hat{\mathbf{p}}_z$ will converge slowly in time. This behavior is illustrated in Figs. 11(a) and 11(c). Conversely, if h_S is known accurately, then (16) implies that p_z can be inferred accurately, as shown in Figs. 10(a) and 10(c).

As expected, the velocity and distance to ground estimate enhancements are independent of the available terrain height information, as seen by comparing Figs. 10(b) and 10(d) with Figs. 11(b) and 11(d), respectively. These results show that the LASER range finder is critical for landing the robotic platform without risking the robotic platform, by allowing for accurate distance-to-ground and vehicle velocity estimates. Position and ground height estimation is also enhanced in the medium term, by combining LASER and GPS measurements.

7. Conclusion

A new embedded methodology to integrate the vehicle dynamics in the navigation system was proposed. The internal VD system accuracy was shown to be equivalent to the classical external vehicle model architecture, but with smaller computational cost and with a flexible choice of vehicle model differential equations. The application of the proposed technique to a highly nonlinear Vario X-Treme helicopter model validated the approach.

Trimming trajectory simulation results showed that the bias calibration errors were quickly compensated and that bias estimates were enhanced. The linear and angular velocity were improved with respect to the classical GPS/INS configuration. Position and attitude errors, although not observable by the VD model, remained bounded. The LASER range finder sensor provided high precision distance-to-ground estimates for takeoff and landing maneuvers. The proposed VD aiding techniques steps forward as a valuable

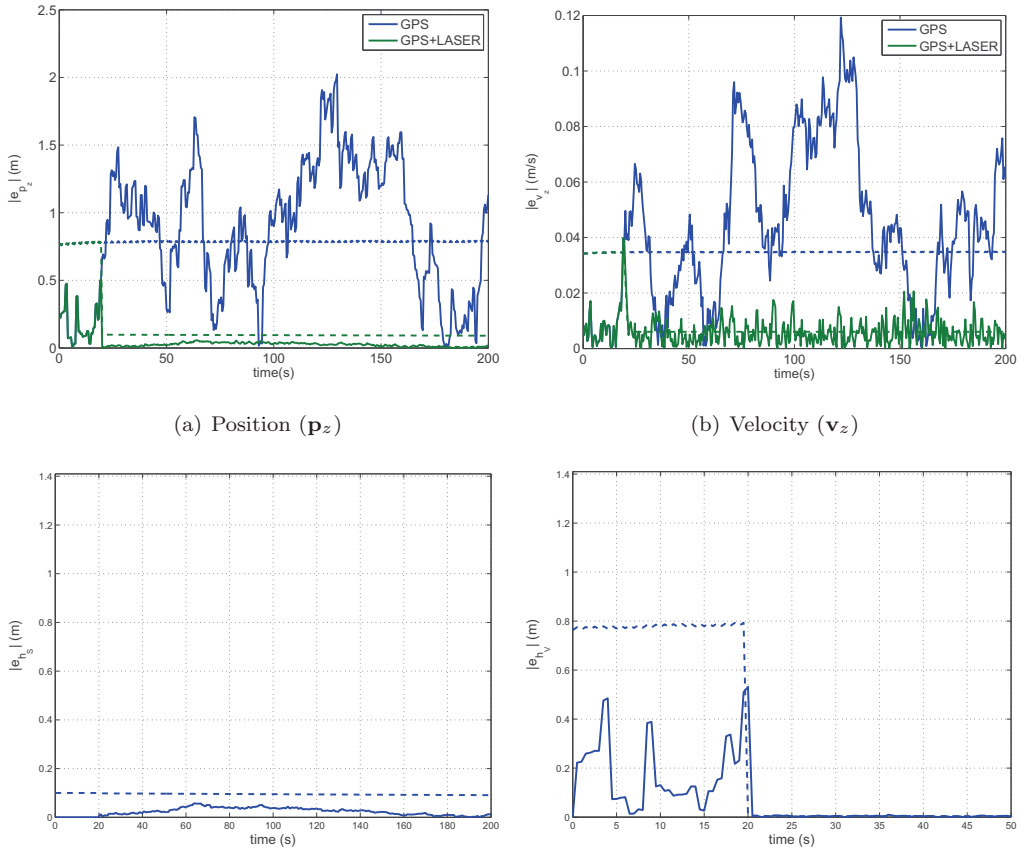

(a) Position ($\mathbf{p}_z$)

(b) Velocity ($\mathbf{v}_z$)

(c) Ground Height (h_S)

(d) Vehicle Height (h_V)

Figure 10: LASER aiding estimation errors (solid line) and estimated error standard deviation (dashed line)

software based technique for navigation systems, suitable for performing critical maneuvers and positioning in scenarios where other sources of aiding information are limited.

Acknowledgments

This work was partially supported by Fundação para a Ciência e a Tecnologia (ISR/IST plurianual funding) through the POS_Conhecimento Program that includes FEDER funds and by the POSI/SRI/41938/2001 ALTICOPTER project. The work of J.F. Vasconcelos was supported by a PhD Student Scholarship, SFRH/BD/18954/2004, from the Portuguese FCT POCTI programme.

A. Helicopter Model Summary

This Section briefly describes the nonlinear Vario X-Treme helicopter model presented in (Cunha and Silvestre, 2003), deduced from first principles, and simplified under the assumptions described in (Guerreiro, 2005).

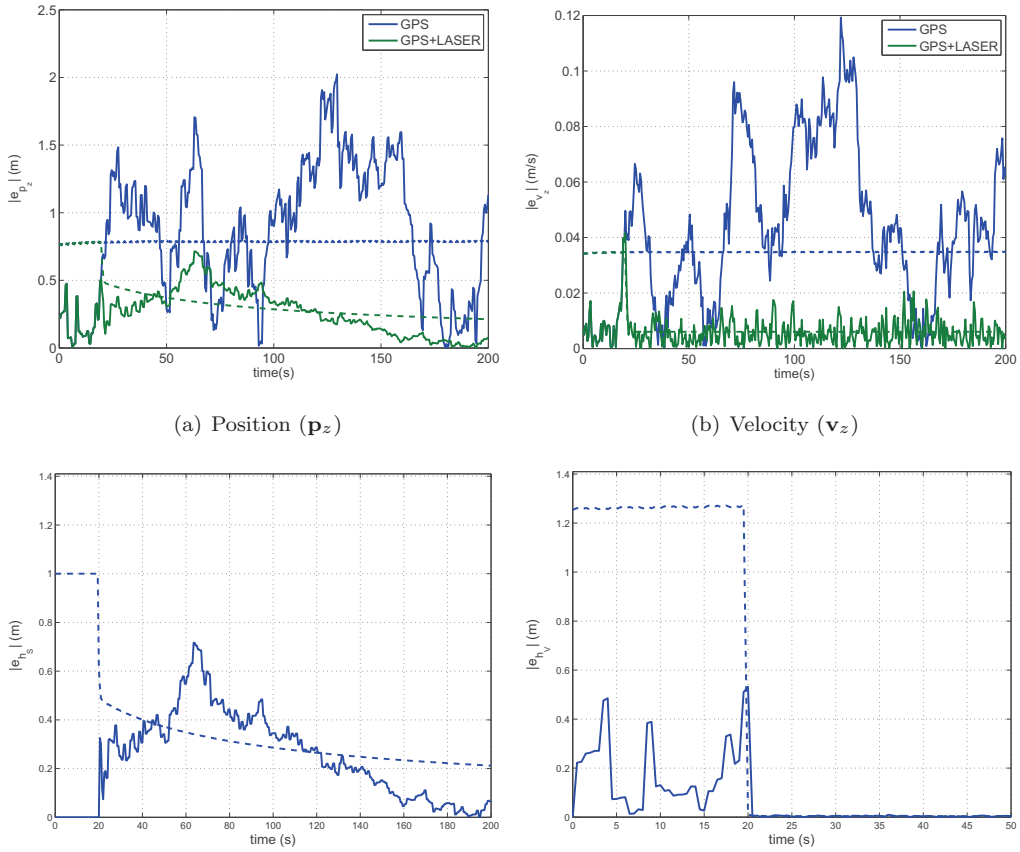

(a) Position ($\mathbf{p}_z$)

(b) Velocity ($\mathbf{v}_z$)

(c) Ground Height (h_S)

(d) Vehicle Height (h_V)

Figure 11: LASER aiding estimation errors (solid line) and estimated error standard deviation (dashed line)

As the complete model, the simplified model considers a six degrees of freedom rigid body dynamics driven by the external forces and moments generated by the several components of helicopter, however, the contributions of the fuselage, horizontal tailplane and vertical tail fin are considered to be negligible. This model also considers simplified versions of the first order dynamics for the main rotor blade pitch motion with Bell-Hiller mechanism, the steady state dynamics for the main rotor blade flap dynamics and the blade lag dynamics are neglected.

The motion of the helicopter is described using the rigid body equations of motion

$$\begin{aligned}
\dot{\boldsymbol{\omega}} &= \mathbf{I}_B^{-1}\left(\mathbf{n}\left(\boldsymbol{\omega}, \mathbf{u}, \mathbf{u}_{hc}\right) - \boldsymbol{\omega} \times \mathbf{I}_B\, \boldsymbol{\omega}\right), \\
\dot{\mathbf{u}} &= -\boldsymbol{\omega} \times \mathbf{u} + \frac{1}{m}\mathbf{f}\left(\boldsymbol{\omega}, \mathbf{u}, \mathbf{u}_{hc}\right) + \mathcal{R}'^{\,E}\mathbf{g}, \\
\dot{\mathcal{R}} &= \mathcal{R}\left(\boldsymbol{\omega}\right)_{\times},
\end{aligned}$$

where m is the vehicle mass, $\mathbf{I}_B$ is the tensor of inertia about the Center of Mass coordinate frame, denoted by $\{G\}$, $\mathbf{u}_{hc}$ is the helicopter command vector and $\mathbf{f}$ and $\mathbf{n}$ are the vectors of external forces and moments,

respectively, along the same frame. The input vector $\mathbf{u}_{hc} = \begin{bmatrix} \theta_{c_0} & \theta_{c_{1c}} & \theta_{c_{1s}} & \theta_{c_{0_t}} \end{bmatrix}'$ comprises the blade pitch angle commands for the main rotor collective θ_{c_0}, main rotor longitudinal cyclic $\theta_{c_{1c}}$, main rotor lateral cyclic $\theta_{c_{1s}}$ and the tail rotor collective $\theta_{c_{0_t}}$. To model the non symmetric shape of the rotor blades, θ_{c_0} and $\theta_{c_{0_t}}$ swashplate inputs are corrected in the helicopter model using the variables $\theta_0 = \theta_{c_0} + \alpha_0$ and $\theta_{0_t} = \theta_{c_{0_t}} + \alpha_{0_t}$, where α_0 and α_{0_t} are the lift curve slope offsets for the main and tail rotor blades, respectively.

As noted before, for smooth low velocity maneuvers, the effects of the fuselage, horizontal tailplane and vertical fin on the overall dynamics are negligible. For this reason, the total force and moment vectors are modeled accounting only for the two most dominant components of a helicopter, the main rotor and the tail rotor, yielding

$$\mathbf{f} = \mathbf{f}_{mr} + \mathbf{f}_{tr}, \qquad \mathbf{n} = \mathbf{n}_{mr} + \mathbf{n}_{tr},$$

where the subscripts mr and tr stand, respectively, for the main rotor and tail rotor components.

The main rotor is the primary source of lift, required to sustain the helicopter, and generates other forces and moments that allow for the control of position, orientation and velocity of the helicopter. The main forces and moments are described by

$$\mathbf{f}_{mr} := \begin{bmatrix} X_{mr} \\ Y_{mr} \\ Z_{mr} \end{bmatrix} = -s_1 \begin{bmatrix} a_0 \left(\frac{1}{2} \theta_{1s} \lambda_0 + \mu \lambda_0 \theta_0 \right) + \delta_0 \mu \\ a_0 \left(\frac{1}{2} \theta_{1c} \lambda_0 \right) \\ a_0 \left(\frac{2}{3} \theta_0 - \lambda_0 \right) \end{bmatrix},$$

$$\mathbf{n}_{mr} = \begin{bmatrix} -k_\beta \beta_{1s} \\ -k_\beta \beta_{1c} \\ \frac{1}{2} s_2 \delta_0 + s_2 a_0 \left(\frac{2}{3} \theta_0 \lambda_0 - \lambda_0^2 \right) \end{bmatrix} + \begin{bmatrix} Y_{mr} h_R \\ -X_{mr} h_R + Z_{mr} x_{cm} \\ -Y_{mr} x_{cm} \end{bmatrix},$$

where s_1 and s_2 are the main rotor's force and moment normalizing constants, a_0 is the lift curve slope, δ_0 is the profile drag coefficient, k_β is the center-spring rotor stiffness, and x_{cm} and h_R determine the position of the main rotor hub aft and above the center of mass, respectively. The remaining undefined variables are defined hereafter.

In helicopters equipped with the Bell-Hiller mechanism (Cunha and Silvestre, 2003), the cyclic blade pitch angles result from the combination of the commands introduced by the swashplate and the flybar flapping motion. The simplified first order blade pitch dynamics of the main rotor are described by

$$\dot{\theta}_{1c} = C_{\theta_1} \theta_{1c} + C_{\theta_3} \theta_{c_{1c}}, \qquad \dot{\theta}_{1s} = C_{\theta_1} \theta_{1s} + C_{\theta_3} \theta_{c_{1s}} + C_{\theta_8} \mu \lambda_0,$$

with the coefficients given by

$$C_{\theta_1} = -\frac{\Omega \gamma_f}{4 \left[\left(\frac{\gamma_f}{8} \right)^2 + 4 \right]}, \quad C_{\theta_3} = \frac{\Omega \left(c_4 + c_1 \right) \gamma_f}{4 c_2 \left[\left(\frac{\gamma_f}{8} \right)^2 + 4 \right]}, \quad C_{\theta_8} = -\frac{\eta_2 \Omega \gamma_f}{2 c_2 \left[\left(\frac{\gamma_f}{8} \right)^2 + 4 \right]},$$

where μ stands for the normalized forward velocity at the main rotor, λ_0 is the normalized collective downwash induced by main rotor, Ω is the main rotor angular speed, γ_f is the flybar lock number, and c_1, c_2 and c_4 are flybar pitching parameters.

The main rotor blade flapping motion is described by the blade flap angle vector $\boldsymbol{\beta} = \begin{bmatrix} \beta_0 & \beta_{1c} & \beta_{1s} \end{bmatrix}$, where β_0 denotes the collective mode, and β_{1c} and β_{1s} represent the longitudinal and lateral cyclic modes, respectively. The blade flapping dynamics of the main rotor can be approximated by the simplified steady-state solution given by

$$\begin{aligned}
\beta_0 &= C_{\beta_1}\,\theta_0, \\
\beta_{1c} &= C_{\beta_3}\,\mu\,\theta_0 + C_{\beta_4}\,\theta_{1c} - C_{\beta_5}\,\theta_{1s} + C_{\beta_6}\,\omega_x + C_{\beta_7}\,\omega_y + C_{\beta_8}\,\mu\,\lambda_0 - C_{\beta_4}\,\lambda_{1c}, \\
\beta_{1s} &= C_{\beta_9}\,\mu\,\theta_0 + C_{\beta_5}\,\theta_{1c} + C_{\beta_4}\,\theta_{1s} + C_{\beta_7}\,\omega_x - C_{\beta_6}\,\omega_y + C_{\beta_{10}}\,\mu\,\lambda_0 - C_{\beta_5}\,\lambda_{1c},
\end{aligned}$$

with the state coefficients

$$\begin{aligned}
C_{\beta_1} &= \frac{\frac{\gamma}{8}}{\frac{\gamma}{8} S_\beta + 1},\ C_{\beta_3} = -\frac{\frac{8}{3}}{S_\beta^2 + 1},\ C_{\beta_4} = \frac{S_\beta}{S_\beta^2 + 1}, \\
C_{\beta_5} &= \frac{1}{S_\beta^2 + 1},\ C_{\beta_6} = \frac{16}{\Omega\,\gamma}\,\frac{S_\beta}{S_\beta^2 + 1},\ C_{\beta_7} = \frac{16}{\Omega\,\gamma}\,\frac{1}{S_\beta^2 + 1}, \\
C_{\beta_8} &= \frac{2}{S_\beta^2 + 1},\ C_{\beta_9} = \frac{\frac{8}{3}\,S_\beta}{S_\beta^2 + 1},\ C_{\beta_{10}} = -\frac{2\,S_\beta}{S_\beta^2 + 1},
\end{aligned}$$

where S_β is the blade stiffness number, R_m is the main rotor radius and γ is the lock number.

The tail rotor, placed at the tail boom in order to counteract the moment generated by the rotation of the main rotor, provides yaw control of the helicopter. Following the same principles used for the main rotor and neglecting blade pitch, flap and lag dynamics, the simplified expressions for the tail rotor force and torque are given by

$$\begin{aligned}
\mathbf{f}_{tr} &:= \begin{bmatrix} X_{tr} \\ Y_{tr} \\ Z_{tr} \end{bmatrix} = s_{1_t}\,a_{0_t} \begin{bmatrix} 0 \\ \frac{2}{3}\,\theta_{0_t} - \lambda_{0_t} \\ 0 \end{bmatrix}, \\
\mathbf{n}_{tr} &= \begin{bmatrix} Y_{tr}\,h_{tr} \\ -\frac{1}{2}\,s_{2_t}\,\delta_{0_t} - s_{2_t}\,a_{0_t}\left(\frac{2}{3}\,\theta_{0_t}\,\lambda_{0_t} - \lambda_{0_t}^2\right) \\ -Y_{tr}\,(x_{cm} + l_{tr}) \end{bmatrix},
\end{aligned}$$

where λ_{0_t} is the collective induced downwash of the tail rotor, s_{1_t} and s_{2_t} are the tail rotor's force and moment normalizing constants, a_{0_t} is the tail rotor lift curve slope, δ_{0_t} is the tail rotor profile drag coefficient, l_{tr} is the distance from the tail rotor hub to the fuselage reference point and h_{tr} is the height of tail rotor hub above the fuselage reference point.

The induced downwash results from the thrust force generated at the surface of the rotating blades, that accelerates the air downwards creating a flowfield. By decomposing the downwash in Fourier series

and neglecting the second and higher order terms, results in the collective, longitudinal and lateral cyclic components, respectively, λ_0, λ_{1c} and λ_{1s}. The collective induced downwash at the main and tail rotors are given by

$$\lambda_0 = -\frac{a_0\, s}{16} + \sqrt{\left(\frac{a_0\, s}{16}\right)^2 + \frac{a_0\, s}{12}\,\theta_0},$$
$$\lambda_{0_t} = -\frac{a_{0_t}\, s_t}{16} + \sqrt{\left(\frac{a_{0_t}\, s_t}{16}\right)^2 + \frac{a_{0_t}\, s_t}{12}\,\theta_{0_t}},$$

where s and s_t are the solidity constants of the main and tail rotors, respectively. Finally, the main rotor longitudinal cyclic induced downwash and the forward normalized velocity are described by

$$\lambda_{1c} = \begin{cases} 0, & \text{if } \mu = 0 \text{ (vertical flight)} \\ \lambda_0 \left(\sqrt{1 + \left(\frac{\lambda_0}{\mu}\right)^2} - \left|\frac{\lambda_0}{\mu}\right| \right), & \text{otherwise} \end{cases},$$
$$\mu = \frac{u_x - h_R \omega_y}{\Omega R_m},$$

whereas the main rotor lateral cyclic downwash is neglected $\lambda_{1s} = 0$, as well as both tail rotor cyclic downwash components.

References

Bar-Itzhack, I., Harman, R., 2003. The effect of sensor failure on the attitude and rate estimation of the map spacecraft. AIAA Guidance, Navigation and Control Conference.

Britting, K., 1971. Inertial Navigation Systems Analysis. John Wiley & Sons, Inc.

Brown, R., Hwang, P., 1997. Introduction to Random Signals and Applied Kalman Filtering, 3rd Edition. John Wiley & Sons, Inc.

Bryson, M., Sukkarieh, S., December 2004. Vehicle model aided inertial navigation for a uav using low-cost sensors. In: Proceedings of the Australasian Conference on Robotics and Automation. Canberra, Australia.

Craig, J., 1989. Introduction to Robotics, 2nd Edition. Addison-Wesley, New York.

Crassidis, J. L., Markley, F. L., Cheng, Y., January-February 2007. Survey of nonlinear attitude estimation methods. Journal of Guidance, Control, and Dynamics 30 (1), 12–28.

Cunha, R., Silvestre, C., 2003. Dynamic modeling and stability analysis of model-scale helicopters with bell-hiller stabilizing bar. AIAA Guidance, Navigation and Control Conference.

Dissanayake, G., Sukkarieh, S., October 2001. The aiding of a low-cost strapdown inertial measurement unit using vehicle model constraints for land vehicle applications. IEEE Transactions On Robotics and Automation 17 (5), 731–747.

Goshen-Meskin, D., Bar-Itzhack, I., October 1992a. Observability analysis of piece-wise constant systems - part i: Theory. IEEE Transactions On Aerospace and Electronic Systems 28 (4), 1056–1067.

Goshen-Meskin, D., Bar-Itzhack, I., October 1992b. Observability analysis of piece-wise constant systems - part ii: Application to inertial navigation in-flight alignment. IEEE Transactions On Aerospace and Electronic Systems 28 (4), 1068–1075.

Guerreiro, B., 2005. Vario x-treme helicopter nonlinear model: Complete and simplified expressions. Tech. rep., Institute for Systems and Robotics.

Guerreiro, B., Silvestre, C., Oliveira, P., Vasconcelos, J., May 2008. Nonlinear and geometric optimization methods for ladar calibration. pp. 1406–1411.

Hegrenaes, O., Berglund, E., Hallingstad, O., May 2008. Model-aided inertial navigation for underwater vehicles. In: Robotics and Automation, 2008. ICRA 2008. IEEE International Conference on. pp. 1069–1076.

Ignagni, M., Summer 1998. Duality of optimal strapdown sculling and coning compensation algorithms. Journal of the Institute of Navigation 45 (2), 85–95.

Julier, S., Durrant-Whyte, H., February 2003. On the role of process models in autonomous land vehicle navigation systems. IEEE Transactions on Robotics and Automation 19 (1), 1–13.

Kinsey, J. C., Eustice, R. M., Whitcomb, L. L., September 2006. A survey of underwater vehicle navigation: Recent advances and new challenges. In: Proceedings of the 7th IFAC Conference of Manoeuvring and Control of Marine Craft (MCMC). Lisbon, Portugal, invited paper.

Koifman, M., Bar-Itzhack, I., July 1999. Inertial navigation system aided by aircraft dynamics. IEEE Transactions on Control Systems Technology 7 (4), 487–493.

Ma, X., Sukkarieh, S., Kim, J., 2003. Vehicle model aided inertial navigation. In: Proceedings of the IEEE Intelligent Transportation Systems. Vol. 2. Shangai, China, pp. 1004–1009.

Markley, F., March-April 2003. Attitude error representations for kalman filtering. AIAA Journal of Guidance, Control, and Dynamics 26 (2), 311–317.

Morgado, M., Oliveira, P., Silvestre, C., Vasconcelos, J., 2007. Vehicle dynamics aiding technique for USBL/INS underwater navigation system. In: Proceeding of CAMS 2007- IFAC Conference on Control Applications in Marine Systems. Bol, Croatia.

Pittelkau, M., November-December 2003. Rotation vector in attitude estimation. AIAA Journal of Guidance, Control, and Dynamics 26 (6), 855–860.

Savage, P., January-February 1998a. Strapdown inertial navigation integration algorithm design part 1: Attitude algorithms. AIAA Journal of Guidance, Control, and Dynamics 21 (1), 19–28.

Savage, P., March-April 1998b. Strapdown inertial navigation integration algorithm design part 2: Velocity and position algorithms. AIAA Journal of Guidance, Control, and Dynamics 21 (2), 208–221.

Vasconcelos, J., Oliveira, P., Silvestre, C., August 2005. Inertial navigation system aided by gps and selective frequency contents of vector measurements. In: Proceedings of the AIAA Guidance, Navigation, and Control Conference (GNC2005). American Institute for Aeronautics and Astronautics, San Francisco, USA.

Vasconcelos, J., Silvestre, C., Oliveira, P., August 2006. Embedded vehicle dynamics and laser aiding techniques for inertial navigation systems. In: Proceedings of the AIAA Guidance, Navigation, and Control Conference (GNC2006). Keystone, CO, USA.